Nuclear Magnetic Resonance Characterization of Solid Polymer Electrolyte Materials

by

Alison L. Michan

BASc, The University of British Columbia, 2005

A THESIS SUBMITTED IN PARTIAL FULFILLMENT OF
THE REQUIREMENTS FOR THE DEGREE OF

MASTER OF APPLIED SCIENCE

in

The Faculty of Graduate Studies

(Engineering Physics)

THE UNIVERSITY OF BRITISH COLUMBIA

(Vancouver)

July 2012

Abstract

Solid polymer electrolytes have the potential to improve manufacturability, performance, and safety characteristics of lithium-ion batteries by replacing conventional liquid electrolytes. Two different solid polymer electrolyte materials were characterized using Nuclear Magnetic Resonance (NMR) techniques. The first material is a result of research efforts on single-ion conducting polymers. The material is intended to combine the high conductivity properties of ionic liquids with lithium cation single-ion conduction. The goal of the synthesis was to produce a polymerized ionic liquid, where crosslinking an anionic monomer (AMLi) with poly(ethylene glycol) dimethacrylate (PEGDM) immobilizes the fluorinated anionic species. Pulsed-field gradient NMR diffusion measurements of the AMLi/PEGDM samples have demonstrated that both the lithium cations and fluorinated anions are mobile and contributing toward conductivity. Therefore, further work is required to successfully immobilize the fluorinated anion in a crosslinked network. The ^{7}Li and ^{19}F diffusion coefficients of the AMLi/PEGDM 40/60 sample were 3.4x10^{-8} cm^2/s and 2.2x10^{-8} cm^2/s at 100°C. The second material incorporates a poly(ethylene oxide) (PEO) conductive block and polyethylene (PE) reinforcement block. The PEO/PEO-b-PE/$LiClO_4$ samples were not intended to be single-ion conducting and materials synthesis aimed to maximize conductivity and mechanical properties. A ^{7}Li diffusion coefficient of ~4x10^{-8} cm^2/s at 60°C was observed. It is expected that the anion would also be mobile and therefore the polymer electrolyte would be a bi-ionic conductor. These samples demonstrated higher ^{7}Li diffusion coefficients at a given temperature and superior mechanical properties for a flexible polymer electrolyte compared to the AMLi/PEGDM samples. Practically, the diffusion measurements of the solid polymer samples are extremely challenging, as the spin-spin (T_2) relaxation times are very short, necessitating the development of specialized pulsed-field gradient apparatus. These results provide valuable insight into the conduction mechanisms in these materials, and will drive further optimization of solid polymer electrolytes.

Preface

The following research includes NMR characterization of solid polymer materials, synthesized by our collaborators. We have collaborated with two different research groups:

- G.T.M. Nguyen, O. Fichet, F. Vidal, and C. Vancaeyzeele from the Laboratoire de Physicochimie des Polyméres et des Interfaces (LPPI), Institut des Matériaux, at the University of Cergy-Pontoise, France.
- W.-H. Zhong and J. Ji from the School of Mechanical and Materials Engineering at Washington State University.

I have completed all of the NMR characterization and analysis presented in this thesis and have mentioned some brief details of their materials preparation in Chapters 3 and 5 and compared my NMR results to their conductivity measurements.

A publication regarding the AMLi/PEGDM material synthesized by the team at Cergy-Pontoise University was accepted for publication in the proceedings of the MRS 2012 Spring Conference. I was the first author of this paper, which describes some of the results that are presented in Chapters 3 and 4.

Table of Contents

Abstract ii

Preface iii

Table of Contents iv

List of Tables vi

List of Figures vii

Acknowledgements ix

Dedication x

1 Introduction 1
- 1.1 Motivation and Introduction to Lithium-ion Batteries 1
- 1.2 Solid Polymer Electrolytes 2
- 1.3 Relating NMR Measurements to Transport Properties of Solid Polymer Electrolytes 8
- 1.4 Previous NMR Studies of Polymer Electrolytes 10
  - 1.4.1 ^{7}Li and ^{19}F PFG NMR Diffusion Studies 10
  - 1.4.2 ^{7}Li NMR Line Width and Relaxation Studies 12

2 Pulsed-Field Gradient (PFG) NMR Overview 14
- 2.1 Translational Diffusion Theory 14
- 2.2 NMR Pulse Sequence Using PFG 16
- 2.3 Gradient Coil Theory, Design, and Implementation 21
- 2.4 Home-built Probe Design and Implementation 25

3 Characterization of AMLi/PEGDM Samples 29
- 3.1 Material Overview 29
- 3.2 Dry Sample Measurements 30
  - 3.2.1 Line Width and Relaxation Measurements 30

3.2.2 Diffusion Measurements 36
3.3 PC Saturated Samples 38
3.3.1 Line Width and Relaxation Measurements 38
3.3.2 Diffusion Measurements 43
3.4 Additional AMLi/PEGDM samples 43

4 Characterization of AMLi/PEGDM w/DCPD Sample . . 46
4.1 Line Width and Relaxation Measurements 46
4.2 Diffusion Measurements 49
4.3 Quantification of Diffusing Species 49
4.3.1 Method and Calibration 49
4.3.2 PEGM/PEGDM/LiTFSI Reference Samples 53
4.3.3 AMLi/PEGDM 20/80 w/DCPD Sample 57

5 Characterization of PEO/PEO-b-PE/$LiClO_4$ Samples . . . 62
5.1 Line Width and Relaxation Measurements 63
5.2 Diffusion Measurements 65

6 Conclusion and Future Work 69

Bibliography 73

List of Tables

2.1 Temperature calibration 27

3.1 Multi-component ^{7}Li transverse relaxation times for a dry AMLi/PEGDM 40/60 sample 34
3.2 Multi-component ^{7}Li relaxation times for a PC saturated AMLi/PEGDM 70/30 sample 40
3.3 Summary of diffusion coefficients measured in PC saturated AMLi/PEGDM X/Y samples 44

4.1 ^{7}Li and ^{19}F PEGM/PEGDM/LiTFSI dry sample relaxation results 55
4.2 Quantities of ions diffusing in PEGM/PEGDM/LiTFSI sample 57
4.3 ^{7}Li and ^{19}F relaxation results of AMLi/PEGDM 20/80 w/DCPD dry sample at 373 K 58
4.4 Summary of dry AMLi/PEGDM 20/80 w/DCPD diffusion coefficients measured at 373K 60

5.1 ^{7}Li relaxation times for PEO/PEO-b-PE/$LiClO_4$ samples . . 64
5.2 Summary of NMR diffusion coefficients of dry PEO/PEO-b-PE/$LiClO_4$ samples up to 60°C 65

List of Figures

1.1 Schematic: Ionic diffusion in a battery cell 2
1.2 Photo: Safety concerns of batteries 3
1.3 Schematic: Impact of ion-pairing and aggregation 4
1.4 Schematic: Ion migration in a single-ion conducting polymer 7
1.5 Correlation times versus T_1 and T_2 9

2.1 Schematic: Diffusion due to random collisions caused by thermal motion 16
2.2 Spin echo PFG pulse sequence diagram 18
2.3 PFGSE pulse sequence diagram 20
2.4 Gradient coil photo and schematic 21
2.5 Resonance driver circuit charging simulation 23
2.6 Resonance driver circuit discharging simulation 23
2.7 Gradient coil calibration 25
2.8 Diagram of NMR probe with temperature set-up (top view) . 26
2.9 Diagram of NMR probe with temperature set-up (bottom view) 27
2.10 Schematic: Experimental set-up for temperature measurements 28

3.1 Structure of AMLi monomer 30
3.2 AMLi/PEGDM 40/60 dry sample ^{19}F and ^{7}Li spectra 31
3.3 AMLi/PEGDM 40/60 T_1 relaxation measurements 32
3.4 AMLi/PEGDM 40/60 correlation times 32
3.5 AMLi/PEGDM 40/60 spectra at -46°C and 35°C 35
3.6 ^{7}Li and ^{19}F PFGSE data and diffusion coefficient fits for AMLi/PEGDM 40/60 at 373 K 37
3.7 AMLi/PEGDM 70/30 PC saturated sample ^{19}F and ^{7}Li spectra 38
3.8 Multi-component relaxation measurements of PC saturated AMLi/PEGDM 70/30 39
3.9 ^{7}Li spectra of PC saturated AMLi/PEGDM 70/30 from an inversion recovery experiment at 10 ms, 100 ms, 200 ms and 5000 ms. 41

3.10 Multi-component relaxation fits of PC saturated AMLi/PEGDM 70/30 obtained by analyzing the Lorentzian and Gaussian components separately. 42
3.11 ^{7}Li and ^{19}F PFGSE data and diffusion coefficient fits for PC saturated AMLi/PEGDM 70/30 at room temperature 44

4.1 AMLi/PEGDM 20/80 w/DCPD dry sample ^{19}F and ^{7}Li spectra 47
4.2 AMLi/PEGDM w/DCPD ^{19}F relaxation measurements . . . 48
4.3 AMLi/PEGDM w/DCPD ^{7}Li relaxation measurements . . . 48
4.4 ^{7}Li and ^{19}F PFGSE data and diffusion coefficient fits for an AMLi/PEGDM 20/80 w/DCPD sample at 373 K 50
4.5 PFGSE measurements of TBAP/PC calibration solution . . . 52
4.6 Structure of LiTFSI 53
4.7 PEGM/PEGDM/LiTFSI ^{7}Li relaxation measurements 54
4.8 PEGM/PEGDM/LiTFSI ^{19}F relaxation measurements 54
4.9 PEGM/PEGDM/LiTFSI quantity diffusion measurements . . 56
4.10 ^{19}F AMLi/PEGDM 20/80 w/DCPD dry sample quantity diffusion measurements at 373 K 59

5.1 PEO/PEO-b(920)-PE/$LiClO_4$ ^{7}Li spectra 63
5.2 ^{7}Li PFGSE measurements of PEO/$LiClO_4$ 65
5.3 ^{7}Li PFGSE measurements of PEO/PEO-b(875)-PE/$LiClO_4$. 66
5.4 ^{7}Li PFGSE measurements of PEO/PEO-b(920)-PE/$LiClO_4$. 66
5.5 ^{7}Li diffusion coefficients of PEO/PEO-b(875)-PE/$LiClO_4$ as a function of temperature 67

Acknowledgements

Thank you to everyone who has supported me in completing this thesis. I am especially grateful to my supervisor, Professor Carl Michal. His mentorship and timely feedback throughout the course of my research enabled me to further pursue my research interests as a PhD candidate. Thank you also to Professor Ronald Dong for his mentorship in the lab, as well as Professor Lawrence McIntosh for teaching me about the fundamentals of NMR. I would also like to thank my colleagues Alan Manning, Shu Han, and Samara Pillay, for their feedback and discussions throughout the last year. Thank you also to Clark Lemke and Andy Reddin who helped orient me with the NMR lab equipment. Although our overlap in the lab was brief, their support was much appreciated. A big thank you is also due to my predecessor Jenny Tso who first implemented the home-built gradient coil I used and modified for my diffusion studies of solid polymer electrolytes.

Dedication

To my husband Juan Mario

Chapter 1

Introduction

1.1 Motivation and Introduction to Lithium-ion Batteries

Lithium-ion batteries are a preferred battery technology for mobile applications and transportation due to their power-to-weight ratio, durability, and high voltage. However, there are still gains to be made in performance and safety, driving research and development for improved technology. Improving battery technology would open up opportunity for wider use in sustainable technologies and applications such as grid storage and electric vehicles. According to a recent market report, Batteries for Electric Vehicles: the U.S. Value Chain[1], materials development is essential for electric vehicle deployment. Additionally, higher energy density batteries could be used for improved mobile devices. Fundamental materials research will enable us to engineer materials leading to improved performance and safety of batteries.

During battery charge and discharge, lithium ions shuttle between the battery electrodes through an electrolyte. In order to optimize battery materials, it is therefore important to understand and optimize ionic transport through individual electrolyte and electrode materials. Lithium ion diffusion through the electrolyte and across the electrode/electrolyte interfaces can limit the steady state current, power output, and overall performance and lifetime of a battery cell.

Figure 1.1 captures ionic diffusion in a battery cell schematic. In a discharging cell, lithium ions are produced at the anode and consumed at the cathode. In the electrolyte, lithium ions migrate due to the electric potential between the anode and cathode and diffuse due to concentration gradients. Additionally, lithium ions diffuse through the porous electrode and active mass particles, as well as through the solid electrolyte interphase (SEI) layer that forms on the surface of the negative electrode.[2] Each of these diffusion processes impact the performance of a battery cell. Ultimately, any potential new battery material needs to be evaluated in the context of a complete system, where all of the interactions and diffusion processes can be accounted

for. However, the electrolyte is one component where large performance and safety gains can be accomplished and substantial research efforts are being placed on its optimization.

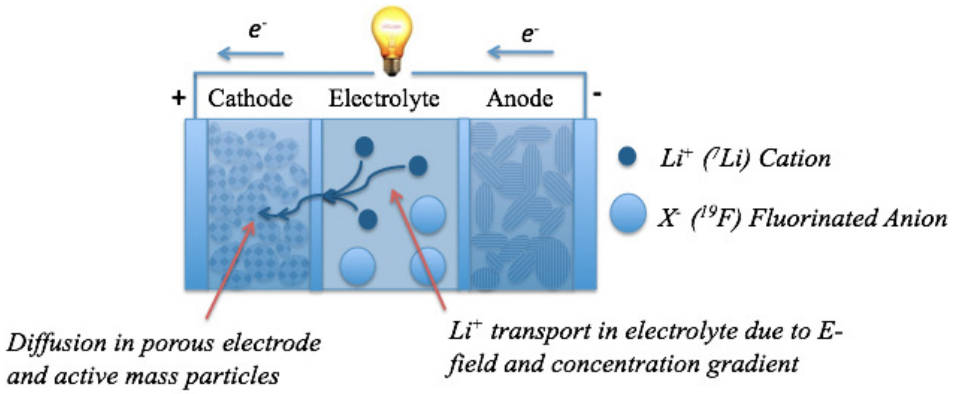

Figure 1.1: Schematic: Ionic diffusion in a battery cell, based on information from Jossen[2]. The battery cell is discharging, powering a light bulb and lithium ions travel from the anode to the cathode to recombine with electrons that travel through the load. Note that the anode and cathode are electrically separated.

In the following study, we concentrate on the isolated electrolyte. In particular, we evaluate two different solid polymer electrolyte materials and investigate the transport properties of the free electrolyte materials using nuclear magnetic resonance (NMR) techniques. The interfacial properties of the material have not been investigated but would also have important practical implications in a complete system.

1.2 Solid Polymer Electrolytes

Solid polymer electrolytes would allow for the construction of fully plastic cells, by replacing conventional liquid or gel electrolytes and separators with a single thin-polymer membrane. This light weight construction would allow for more durable, safe, and easily manufactured battery cells, with high energy density and long lifetime. These advantages would help improve a technology where recalls are common.

In particular, solid polymers have the potential to improve lithium-ion battery safety by replacing conventional liquid electrolytes with a non-

volatile alternative. There is currently a relatively high incident rate of lithium-ion battery failures due to overheating and combustion. As a result, several battery recalls have been issued in recent years. A particularly high profile incident in 2006 involved the recall of Sony manufactured battery cells implemented in Dell and Apple laptops.[3–5] The cost of the recall to Sony was estimated between $170 and $250 million and affected 4.1 million Dell laptops and 1.8 million Apple laptops.[6] The recall was issued due to overheating batteries causing flames and fire, personal property damage, and minor personal injury. Two recent examples of lithium-ion battery fires are captured in Figure 1.2. The first photo is of three flaming 24 V lithium

Figure 1.2: Batteries with flammable electrolyte can cause serious fire and damage and are a key motivator in the development of solid polymer electrolytes as an alternative to conventional liquid and gel electrolytes. (left) Three flaming 24 V flaming polymer gel battery packs that began combusting during use on an electric bicycle. (right) The remains of the author's door after a house fire caused by a 36 V lithium manganese battery and charger.

polymer gel battery packs. The packs were connected in parallel and one of them suddenly combusted during use on an electric bicycle. They were subsequently thrown to the ground to avoid injury. The second photo is the remains of the author's door after a house fire, caused by a 36 V lithium manganese battery pack and charger. No injury was caused by the fire. However, the personal property damage was extensive. Incidents like these are a key motivation for the author's research of solid polymer electrolytes.

In the majority of lithium ion batteries used today, $LiPF_6$ salts are utilized in liquid electrolytes and provide a conductivity on the order of 10^{-3} S/cm.[7] Typical solvents include a combination of ethylene carbonate (EC), propylene carbonate (PC), dimethyl carbonate (DMC), ethyl methyl carbonate (EMC) and diethyl carbonate (DEC). In order to practically implement a battery cell with a solid polymer electrolyte, the material must have transport properties similar to those of liquid electrolytes.[8] The total conductivity of a polymer is given by the sum of the contributions from each of the ionic species i by [9]

$$\sigma = \sum_i n_i q_i \mu_i \tag{1.1}$$

with n the number of charge carriers, q their charge, and μ their mobility. Several opposing factors make it difficult to maximize conductivity in solid polymer materials. For example, amorphous polymers with a low glass transition temperature T_g (the temperature a solid polymer becomes brittle on cooling or soft on heating[10]) maximize ionic mobility μ. However, the formation of ion pairs $[LiX]^\circ$ in these amorphous polymers reduces the concentration of charge carriers and therefore conductivity.[8] The reduction of charge carriers n due to ion pairing is captured in the schematic of Figure 1.3. Ion pairing forms neutrally charged groups $[LiX]^\circ$ that do not migrate due to the electric field between the electrodes.

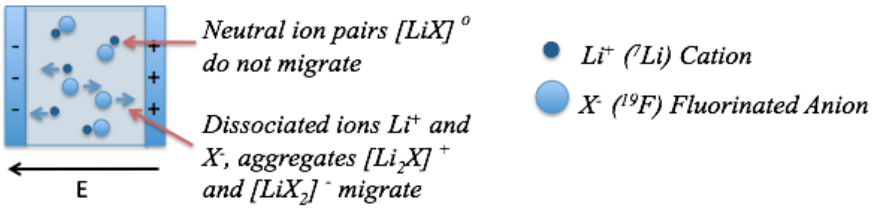

Figure 1.3: Schematic demonstrating effects of ion pairing and aggregation in a battery electrolyte.

Another important aspect to consider in optimizing conductivity in solid polymer materials is operating temperature. Their conductivity must be optimized at a suitable temperature for the application of the particular battery cell. For example, desirable temperatures could range from -40°C to 55°C for the case of an electric vehicle operating in the winter and summer months of North America. Therefore, solid polymers must have a low glass

transition temperature in order to be practically implemented, at least below room temperature for the majority of applications. As an aside, solid polymer electrolytes could be particularly beneficial in high temperature applications to eliminate the need for battery cooling systems. Finally, techniques used to increase conductivity can simultaneously have a negative impact on mechanical strength.[11] The final mechanical strength is therefore also an important consideration when optimizing conductivity.

The total conductivity arises from the sum of the cationic and anionic contributions. The total molar conductivity can be written as

$$\Lambda = \lambda_+ + \lambda_- \,. \tag{1.2}$$

Individual contributions to the total current differ because anions and cations can travel at different speeds under the same potential gradient due to size and solvation.[12] The transport number (or transference number), t_i is defined as the fraction of the total current flowing in an electrolyte phase that is carried by a particular ion, i.[10] The sum of the cationic transference number t_+ and anionic transference number t_- is unity:

$$1 = t_- + t_+ \,. \tag{1.3}$$

We will not be calculating transference numbers using our NMR results, however, it is an important design parameter in the solid polymer electrolyte samples in our investigation so we will introduce some main concepts. In lithium-ion battery cells it is important to maximize the lithium ion transference number because a low transference number is associated with large concentration gradients.[12] As lithium ions are consumed at the cathode and produced at the anode, concentration gradients form near the electrodes. These concentration gradients reduce battery cell performance because they reduce the voltage potential across the electrolyte, steady state current, and therefore power output.[13, 14]

In thin-film solid polymers the negative effects of concentration gradients are especially pronounced compared to liquid electrolytes because convection is absent.[15] In the steady state, large concentration gradients can extend across the thickness of the thin-film solid polymer. As described by Bruce et al[13, 14] and Golodnitsky[15], the anions carried to the cathode in positively charged aggregates such as $[Li_2X]^+$ migrate toward the anode after the Li^+ is consumed in the cathode reaction. Anions also diffuse in the opposite direction toward the cathode, down the concentration gradient. In the steady state, anionic diffusion matches anionic migration in the opposite direction. Therefore, current is only due to cationic diffusion and migration.

The voltage potential due to the gradient causes a reduction from the initial cell potential. As the potential is reduced, there is a reduction in migration and increase in diffusion due to the steeper concentration gradient. In this case, the steady state current I_s^+ is proportional to the lithium ion diffusion coefficient D_+ [14, 15]:

$$I_s^+ = -2FD_+(c_a - c_c)\,, \tag{1.4}$$

where c_a and c_c are the salt concentrations (mol/L) at the anode and cathode and F is Faraday's constant. The steady state current in a solid polymer can therefore be limited by diffusion. The meaning of the diffusion coefficient is described in Chapter 2.

We can obtain an expression in terms of the diffusion coefficients by starting with an expression for the transference number in terms of the molar conductivities and then using the Nernst-Einstein relation. In an infinitely dilute solution, with cations and anions in equal ratio of 1:1, the cationic transference number can be written in terms of the molar conductivities as [12]

$$t_+ = \frac{\lambda_+}{\lambda_+ + \lambda_-}\,. \tag{1.5}$$

Practically, ion association, ion-ion interaction and solvation impact the transference number. It is therefore solvent and concentration dependent. Neutrally charged ion-pairs [LiX]° do not impact the transference number.[15]

Using the Nernst-Einstein relation, we relate the transference number to diffusion coefficients D_- and D_+. The relation is applicable in an infinitely dilute solution with fully dissociated ions. It states the relationship between the conductivity and diffusion coefficients is [8]

$$\Lambda = \frac{\sigma}{C} = \frac{N_A\, e^2}{kT}(D_+ + D_-)\,, \tag{1.6}$$

where D_+ and D_- are the diffusion coefficients of the cation and anions, N_A is Avogadro's number, C is the molar concentration of ions, k is Boltzmann's constant, e is the electron charge and T is the temperature. From this relationship, it follows that the transference number is related to the diffusion coefficients by

$$t_+ = \frac{D_+}{D_+ + D_-}\,. \tag{1.7}$$

A low transference number results in a steep concentration gradient[15] in our solid polymer electrolytes. The lithium transference number should

therefore be maximized, up to the ideal limit of $t_+ = 1$ to prevent the performance reducing concentration gradients.[12]

One strategy to increase the transference number is to immobilize the anionic component so that only the cationic component contributes toward conductivity. Materials implemented using this strategy are called single-ion conducting polymer electrolytes and would ideally have transference numbers of $t_+ = 1$ and $t_- = 0$. These materials would have significantly higher transference numbers than electrolytes utilizing $LiPF_6$ salts in liquid electrolytes, typically less than 0.5.[7] A schematic in Figure 1.4 demonstrates how the immobilized anionic components would be fixed in the electric field between the electrodes of a battery cell.

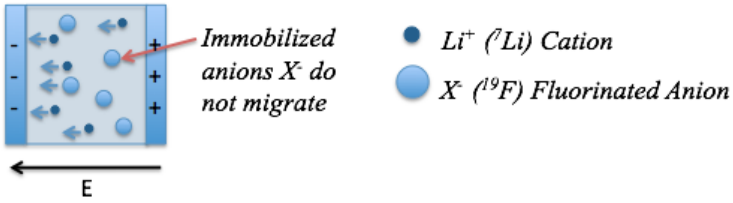

Figure 1.4: Schematic: Ion migration in a single-ion conducting polymer. The positively charged cations are mobile and can therefore migrate due to the electric field between the electrodes. However, the negatively charged anions are immobilized in the material.

The high transference number of single-ion conducting electrolyte materials would help reduce concentration gradients. However, one drawback with these materials is that the number of charge carriers is reduced, as only the cations are mobile. Therefore, the challenge with these materials is to simultaneously increase conductivity. One route to success would combine the properties of ionic liquids and single-ion conducting polymers. Ionic liquids are liquids that contain only ions.[10] They have relatively high conductivity at room temperature and also have negligible vapour pressure. Therefore, a strategy of producing single-ion conducting polymers by polymerizing ionic liquids is expected to produce solid polymer electrolytes with high conductivity.

The optimization of the single-ion conducting polymer materials examined here has been aimed at increasing the t_+ number, among other characteristics. Our task is to examine the extent to which this has been accomplished. Our approach is to characterize the materials by looking at their diffusion characteristics using NMR techniques.

1.3 Relating NMR Measurements to Transport Properties of Solid Polymer Electrolytes

Using NMR we can uniquely measure individual cationic and anionic species to gain insight into ionic transport in solid polymer electrolyte materials. We can probe translational diffusion scales on the order of microns over a (greater than ~100) ms timescale in order to measure self-diffusion coefficients. Our measurements of the self-diffusion coefficients are ex situ, so the diffusion coefficients (described in Chapter 2) arise due to thermal motion. For a transference number of unity, we can see from Equation 1.7 that the condition on the diffusion coefficients of $D_+ >> D_-$ arises. By measuring and comparing diffusion coefficients of the anionic and cationic nuclear species we can confirm if a material is single-ion conducting.

NMR measurements include contributions from neutral ion pairs, so if NMR diffusion coefficients are used to calculate transference numbers, they may differ from the transference number measured by other methods because neutral ion pairs do not practically influence the transference number (neutral ion pairs do not migrate due to an applied E-field). Thus, transference numbers calculated from NMR results are accurate only for fully dilute systems where ions are fully dissociated.[15] Similarly, conductivity estimates computed from the Nernst-Einstein equation

$$\Lambda = \frac{\sigma_{NMR}}{C} = \frac{N_A\, e^2}{kT}(D_+ + D_-)\,, \tag{1.8}$$

will also deviate from the measured conductivity. However, the ratio of measured conductivity using AC measurements, σ_{exp}, to the conductivity calculated with the Nernst-Einstein equation using NMR measured diffusion coefficients, σ_{NMR}, can be used as a rough approximation of the degree of dissociation in the material.[8, 16] Reduced dissociation indicates the degree of ion pairing or aggregation reducing the number of effective charge carriers, as discussed previously.

There are several methods to calculate transference numbers and conductivity such as methods using AC and DC measurements.[15] However, NMR particularly excels at differentiating between anionic and cationic species. NMR diffusion measurements are therefore an excellent method in confirming if the anionic species is successfully immobilized. Furthermore, we can characterize materials properties through NMR relaxation measurements and spectra. Specifically, we will gain insight into ionic mobility and uniformity in solid polymer electrolyte samples over a range of temperatures.

One technique we can use to gain insight about ionic mobility in short range motion on the ps-ns timescale (compared to diffusion measurements that characterize ionic mobility of long-range motion on the ms timescale) is to examine NMR longitudinal and transverse magnetization decays, that are characterized by relaxation decay constants T_1 and T_2. Levitt defines relaxation as the process by which thermal equilibrium is regained (after an applied RF pulse) through interaction of the spin system with the thermal molecular environment.[17] Relaxation times are determined by motional processes of the measured nuclei (^{7}Li and ^{19}F in our study) and by comparing their values we can understand the mobility of the corresponding nuclei. T_1 is due to fluctuations in local fields on the timescale of the resonance frequency, while T_2 has contributions from both fluctuations at the resonance frequency as well as static local fields.

The relaxation decay constants T_1 and T_2 are dependent upon the correlation time, τ_c, a quantitative measure of the rate of molecular motion. It is roughly the time of a jump or molecular reorientation.[18] The relationships between T_1 and T_2 with correlation time for many common relaxation processes are shown schematically in Figure 1.5.

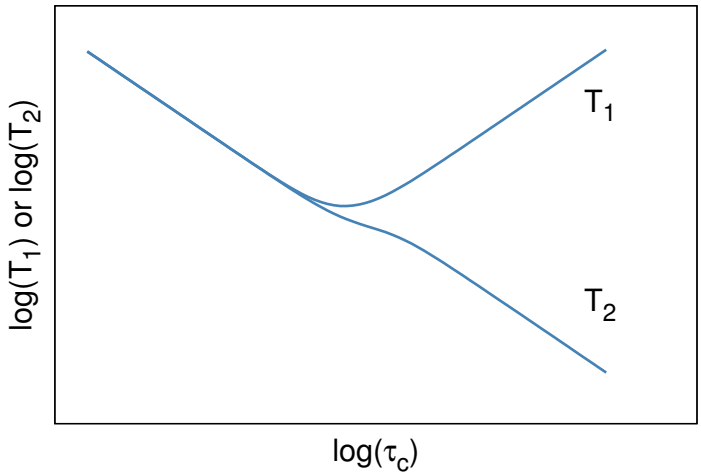

Figure 1.5: Schematic of the variation of the relaxation rates T_1 and T_2 as a function of τ_c. Standard T_1 and T_2 relaxation expressions, which depend on τ_c and ω_o, are plotted. At the T_1 minimum $1 = \omega_o \tau_c$.

In Figure 1.5 the short correlation times where T_1=T_2 correspond to a small molecule in a non-viscous liquid.[17] In the opposite regime, longer correlations times with short T_2 times and long T_1 times correspond to large molecules and viscous liquids. T_2 levels off in the rigid lattice limit.[19] These regimes correspond to narrow and broad line widths because the line widths are inversely proportional to T_2 decay times. In our solid polymer samples, for highly mobile nuclei contributing toward conductivity we expect T_1>T_2 in the mid region of the schematic, near the T_1 minimum. We do not expect these materials to be in the solid regime on the right side of the schematic where $T_1 \gg T_2$.

If we would like to calculate the relation between τ_c and the relaxation times precisely, all of the types of interactions and types of motion must be accounted for. Quadrupolar relaxation (as in the case for ^{7}Li where I=3/2) differs from Figure 1.5 in the long correlation time limit. However, the overall dependence of relaxation times on correlation time is captured in the schematic.

There is an abundance of literature on relaxation theory that we will draw from in our analysis including Abragam's text[20] and this brief discussion serves as a high level introduction for our relaxation time analysis of the solid polymer electrolyte materials.

1.4 Previous NMR Studies of Polymer Electrolytes

Solid polymer electrolyte materials have been investigated since the 1970's.[14] Previous investigations of the transport properties of polymer electrolytes will be used for comparison in our study. First, we will discuss ^{7}Li and ^{19}F pulsed-field gradient (PFG) NMR studies to characterize long-range diffusion.[16, 21, 22] (PFG measurement methods are discussed in Chapter 2) Next, we will discuss ^{7}Li investigations of short-range motions through line width and relaxation measurements.[23–25] Long-range cationic transport can be modelled as a combination of local segmental motions and independent transitions of ions between coordination sites that may be on different polymer strands.[21]

1.4.1 ^{7}Li and ^{19}F PFG NMR Diffusion Studies

Studies by Arumugam et al [21], Williamson et al [22], and more recently, Chauvin et al [16], have used ^{7}Li and ^{19}F PFG NMR to characterize ionic

transport in polymer electrolytes. Each of these studies have measured diffusion coefficients of cationic and anionic species and used the Nernst-Einstein Equation 1.8 for comparison to AC conductivity measurements. Through the comparison of σ_{NMR} to σ_{exp}, the extent of ion pairing and percent dissociation were investigated.

Arumugam et al [21] characterized mechanisms of ionic transport and measured diffusion of Li^+ and PF_6^- -based species in an amorphous polymer electrolyte using PFG NMR. A gradient up to 4 T/m (400 G/cm) and diffusion times up to 900 ms were used to study electrolytes with a range of concentrations of ethylene oxide to salt molar ratios up to temperatures of 100°C. For a polymer electrolyte with ethylene oxide to salt molar ratio of 50:1 the anionic diffusion coefficient was found to be $3.7x10^{-7}cm^2/s$, that was significantly faster than the diffusion coefficient of $0.58x10^{-7}cm^2/s$ for lithium based species at 90°C. At room temperature, they found the anionic diffusion coefficient was two orders of magnitude faster than the lithium based species. Furthermore, they demonstrated σ_{NMR} overestimated σ_{exp} up to an order of magnitude. The failure of the Nernst-Einstein relationship 1.8 was attributed to ion pairing and the diffusion of neutral ion pairs.

Williamson et al [22] used ^7Li and ^{19}F PFG NMR to study ionic mobility in model polymer electrolyte solutions of tetraethylene glycol dimethyl ether/$LiCF_3SO_3$ and N,N dimethyl formamide/$LiCF_3SO_3$. They measured diffusion coefficients over a range of concentrations and temperatures from 35°C to 80°C. They found the cationic and anionic species Li^+ and $CF_3SO_3^-$ had close correspondence over the temperature ranges and suggested their motion must be correlated. They used the Nernst-Einstein equation to compare their measurements to conductivity in order to examine the extent of ionic association and found σ_{NMR} overestimated conductivity by up to an order of magnitude.

More recently Chauvin et al [16] have used NMR to characterize mixed polymer electrolytes based on lithium trifluoromethylsulfonylimide (LiTFSI) and lithium oligoether sulfates dissolved in poly(oxyethylene) (POE). A gradient strength up to 55 G/cm and diffusion time of 500 ms were used. Cationic Li^+ transference numbers ranged from 0.22 to 0.33, determined by AC and DC measurement methods. Diffusion coefficients of ^{19}F anions were found to be on the order of 10^{-7} cm^2/s and ^7Li on the order of $5x10^{-8}$ cm^2/s at 346 K. Percent dissociation was estimated by comparing the NMR estimated conductivities to those calculated by the Nernst-Einstein equation.

1.4.2 ^{7}Li NMR Line Width and Relaxation Studies

Studies by Panero et al [23], Adamic and Greenbaum [24], and Croce [25] have used ^{7}Li NMR to study short-range motions and ionic mobility in polymer electrolytes. Each of these studies have examined NMR line widths and T_1 longitudinal relaxation through polymer glass transition temperatures T_g.

Panero et al[23] have completed an ionic conductivity and ^{7}Li NMR study of (viscous liquid) poly(ethylene glycol) (PEG) complexed with lithium salts. The ^{7}Li NMR measurements were employed to probe the immediate environment of the lithium cations through T_g, and characterize the polymer segmental motions giving rise to ionic mobility. Measurements showed ^{7}Li spectra below T_g consisted of a narrow central peak of approximately 6.7 kHz full width at half maximum (FWHM) superposed on a broader peak of approximately 30 kHz FWHM. Onset of motional narrowing of the central peak was approximately at T_g, consistent with the role of polymer segmental motion in determining ionic conductivity. T_1 relaxation measurements over a range of temperatures were found to be describable by a single exponential. Of three samples measured, the lowest T_1 minimum was also the sample with the lowest T_g where the dominant relaxation mechanism was attributed to quadrupole interactions (due to fluctuating electric field gradients).

Adamic and Greenbaum[24] completed a ^{7}Li NMR study of polymer electrolyte films to investigate the distribution and temperature-dependent mobility of lithium cations in poly[bis((methoxyethoxy)phosphazene](MEEP) /poly(ethylene oxide)(PEO) composites containing lithium salts. The ^{7}Li spectra showed a narrow peak superposed on a broad component, above T_g. For a MEEP/PEO:$LiClO_4$ sample with T_g of -54°C the broad and narrow components had FWHM peak widths of approximately 4 kHz and 0.8 kHz at -22°C. At 27°C the broad and narrow components had approximate peakwidths of 2 kHz and <1 kHz while at cooler temperatures of -42°C and -73°C the spectra appeared as a single broad peak, with FWHM of approximately 4.8 kHz and 8 kHz. The two components had differing T_1 relaxation times. The broad component was attributed to a crystalline region and the narrow component associated with an amorphous phase. Their interpretation was supported by the disappearance of the spectral component assigned to the crystalline phase above 60°C, the melting point of crystalline PEO. Onset of motional narrowing of the central peak was observed to correspond to Tg, corresponding to segmental motions associated with the rubbery phase necessary for ionic transport.

Croce et al[25] completed a ^{7}Li NMR and ionic conductivity study of gel electrolytes based on poly(acrylonitrile) (PAN). Near Tg, the spectra consisted of a narrow peak superposed on a broad peak. The broad Gaussian component was attributed to a distribution of quadrupole satellite transitions associated with a heterogeneous lithium nearest-neighbour configuration in the composite material. At elevated temperatures, the broad component collapsed and motional narrowing was observed in the central peak. The correspondence between T_g and the onset of ^{7}Li motional narrowing emphasized the coupling between ionic and polymer segmental mobility. The line width at elevated temperatures was approximately 300 Hz above 300 K, attributed to magnetic dipole-dipole interactions of Li^+ with the PAN polymer matrix.

Chapter 2

Pulsed-Field Gradient (PFG) NMR Overview

Using PFG NMR we can quantify translational diffusion of individual cationic and anionic species in a polymer electrolyte material by measuring diffusion coefficients. First, we will discuss the meaning of the diffusion coefficients resulting from our NMR measurements, and how these coefficients relate to translational diffusion. Next, we will briefly discuss NMR pulse sequences used to measure diffusion coefficients, with a focus on the PFG stimulated echo (PFGSE) sequence used on our solid polymer samples. This discussion is followed by details of the gradient coil required to produce a spatially varying magnetic field that is utilized in the PFGSE pulse sequence. Finally, a description of our temperature apparatus is presented, with details of the components added to a home-built probe in order to perform measurements at elevated temperatures.

2.1 Translational Diffusion Theory

The following discussion of translational diffusion draws from introductions to PFG NMR by Callaghan[26], Johnson[27], and Price[28]. Aspects of their derivations are included to provide context for diffusion equations relevant to our measurements of solid polymer electrolytes.

Beginning with Fick's first law, we can see the particle flux $\mathbf{J}$ is proportional to a concentration gradient times the diffusion coefficient D

$$\mathbf{J} = -D\nabla n(\mathbf{r}, t)\,, \tag{2.1}$$

where $n(\mathbf{r}, t)$ is the local concentration of particles. Conservation of mass requires that the flux divergence be equal to the time rate of change of the concentration of particles by

$$-\nabla \cdot \mathbf{J} = \frac{\partial n}{\partial t}\,. \tag{2.2}$$

Combining Equations 2.2 and 2.1 leads to Fick's second law, the diffusion equation,

$$\frac{\partial n}{\partial t} = D\nabla^2 n\,, \tag{2.3}$$

that describes how particles drift from higher to lower concentrations to equalize concentration gradients by mutual diffusion.[26] As Callaghan describes [26], Einstein introduced the idea of self-diffusion [29] driven by random motions of particles due to thermal energy, where no macroscopic concentration gradient exists. The case of self-diffusion arising from thermal motions, instead of a macroscopic concentration gradient, applies to our NMR measurements of solid polymer electrolytes. We will take the term diffusion coefficient to mean self-diffusion coefficient for the remainder of this thesis.

Fick's laws were extended to the application of a locally structured concentration of particles $n(\mathbf{r}, t)$, leading to an expression for the self-diffusion coefficient

$$D = \frac{k_B T}{\zeta} = \frac{k_B T}{6\pi\eta R}\,, \tag{2.4}$$

known as the Sutherland-Einstein relation[26], with Stokes drag $\zeta = 6\pi\eta R$ for a spherical particle of radius R and viscosity η. Diffusion coefficients in our solid polymer are therefore related to molecular size, temperature, and viscosity.

In our polymer samples with no macroscopic concentration gradient, we are interested in the probability of particles moving to r from r_o in time t. Applying Fick's Law 2.3 to the probability density $P(\mathbf{r}_o|\mathbf{r}, t)$ instead of $n(\mathbf{r}, t)$ [26] gives

$$\frac{\partial P(\mathbf{r}_o|\mathbf{r}, t)}{\partial t} = D\nabla^2 P(\mathbf{r}_o|\mathbf{r}, t), \tag{2.5}$$

valid for an isotropic medium, where the diffusion is a simple scalar property. An initial condition at $t = 0$ of $P(\mathbf{r}_o|\mathbf{r}, 0) = \delta(\mathbf{r} - \mathbf{r}_o)$ leads to a solution with a Gaussian dependence on the displacement $(\mathbf{r} - \mathbf{r}_o)$ and time t of

$$P(\mathbf{r}_o|\mathbf{r}, t) = (4\pi D t)^{-3/2} \exp\left(-\frac{(\mathbf{r} - \mathbf{r}_o)^2}{4Dt}\right)\,. \tag{2.6}$$

From Equation 2.6, it follows the average square displacement is related to the self-diffusion coefficient by

$$< (r' - r)^2 >= 6Dt\,, \tag{2.7}$$

and

$$< (x' - x)^2 >= 2Dt\,, \tag{2.8}$$

for an isotropic medium with unrestricted diffusion, which applies to our solid polymer samples. Therefore diffusion coefficients arise from an averaged translational distance travelled in diffusion time t by a particular nuclear species. Using Equation 2.7, we can compute the average distance travelled from the measured diffusion coefficient. For our solid polymer samples, the average translational distance must be within the limit of the width of the samples, as restricted conditions would apply if ionic species were in contact with the edges of the sample. The random walk of a particle due to collisions is described in Figure 2.1. Before collisions occur, the motion of the particle is ballistic. After time t where enough time has passed for collisions to occur, the motion of the particle is diffusive and Equation 2.8 holds.

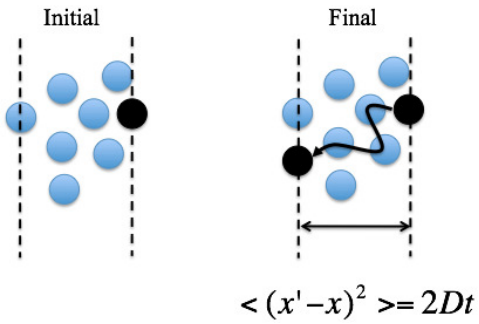

Figure 2.1: Unrestricted diffusive behaviour of a particle due to random collisions caused by thermal motion. The average square distance travelled in time t is proportional to its diffusion coefficient.

2.2 NMR Pulse Sequence Using PFG

Next we discuss how the well-known spin echo and stimulated echo NMR pulse sequences can be combined with pulsed magnetic field gradients to measure diffusion coefficients. General theory of how a spatially varying gradient field affects Larmor precession rates is followed by a description of the PFG NMR pulse sequences, with a focus on the PFG stimulated echo sequence, PFGSE, used to measure ^{7}Li and ^{19}F diffusion coefficients in our solid polymer samples. Basic principles of NMR are not discussed in this thesis, as there is an abundance of literature on the subject. Readers are referred to textbooks by Duer[30], Keeler[31], and Levitt[17] for introductory

material.

The Larmor precession rate of a nucleus in the sample is proportional to the applied magnetic field and its gyromagnetic ratio γ according to

$$\omega(z) = \gamma B_o + \gamma(g \cdot z)\,, \tag{2.9}$$

where the spatially varying magnetic field $g \cdot z$ is added to the static magnetic field of the spectrometer B_0. Thus, the Larmor precession rate of a particle in a sample will depend on the position of the particle along the z axis. Across the sample of radius r, the difference in Larmor precession rates (in Hz) is therefore

$$\Delta\nu = \frac{\gamma g 2r}{2\pi}\,. \tag{2.10}$$

The different precession rates result in a phase accumulation according to

$$\phi(z) = \gamma g z t \tag{2.11}$$

for a rectangular gradient pulse, where the time t is a measure of how long the gradient field is applied. For a time-varying gradient g(t), the expression for phase accumulation would depend on the integral of g(t). The applied gradient field causes a helix of magnetization to wind, due to differences in Larmor precession rates of isochromats along z. Isochromats describe localized sub-ensembles of spins labelled by a single Larmor frequency.[26] The applied gradient therefore causes the net transverse magnetization in the x-y plane to decay.

The Stejskal and Tanner pulsed field gradient (PFG) spin echo experiment [32] is illustrated in Figure 2.2. The Hahn spin echo pulse sequence [33] refocuses our signal and eliminates signal attenuation caused by dephasing in an inhomogenous static field. A pair of gradient pulses is used to encode and decode the position of nuclei in the sample and signal attenuation in the re-focused signal is dependent upon the diffusion coefficient.

In the pulse sequence, initial equilibrium magnetization (aligned along the z-axis with the static magnetic field) is aligned in-phase along the y-axis (in a rotating frame) by a $\pi/2$ pulse. Subsequently, the uniform rectangular shaped gradient pulse is applied that causes a helix of magnetization to wind. A π pulse is then applied which causes the magnetization to flip 180° over the x-axis. The nuclei then precess in the magnetic field in the same direction causing the helix of magnetization to unwind with the second application of the gradient pulse applied with equal strength and equal time duration. At the end of the spin echo experiment, we would expect the signal to be refocused according to Equation 2.11 if the precession rates

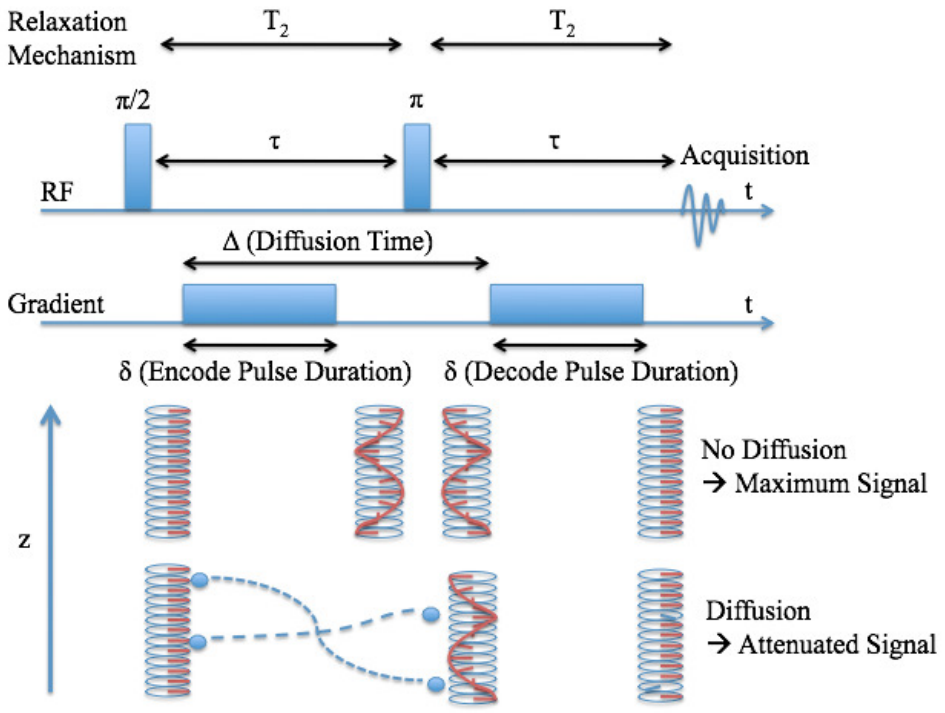

Figure 2.2: Spin echo PFG pulse sequence. In the case of diffusion, the final echo intensity is attenuated due to translational motion of nuclei. Adapted from Callaghan[26], Johnson[27], and Price[28].

of the nuclei are constant, which is the case if the location of the nuclei are fixed along the z-axis. However, movement of nuclei along the z-axis caused by diffusion results in a measurable signal attenuation. Note that in either case, the intrinsic spin-spin T_2 relaxation causes irreversible signal attenuation, not re-focused in the spin-echo experiment. Attenuation caused by T_2 relaxation has important consequences in materials with extremely short T_2 times, discussed in detail below. An expression for the signal intensity of the echo at time $t = 2\tau$ [28] is

$$S(2\tau) = S(0)\ \exp\left(\frac{-2\tau}{T_2}\right) f(\delta, g, \Delta, D), \tag{2.12}$$

where the signal intensity at $t = 0$ is multiplied by an exponential signal attenuation factor due to T_2 relaxation, and an attenuation factor due to diffusion. The diffusion factor is a function of the gradient pulse strength g and duration δ, diffusion time Δ, and diffusion coefficient D. Performing the experiment with a constant time parameter τ, the relaxation effect is constant, leading to

$$\frac{S(2\tau)_{g(b)}}{S(2\tau)_{g=0}} = f(\delta, g, \Delta, D) = e^{\,-bD}, \tag{2.13}$$

where the expression for b depends on the gradient pulse applied.

We have used the example of rectangular pulsed gradients. However, a pair of sinusoidal gradient pulses can also be used which has advantages in implementation for our experiments, discussed in section 2.3. For a pair of sinusoidal gradient pulses, the analytical expression for b derived by Mattiello [34] is given by

$$b = \frac{4}{\pi^2}\gamma^2 G^2 \delta^2 \left(\Delta - \frac{1}{4}\delta\right), \tag{2.14}$$

where the pulses are applied for a duration of δ, separated by a diffusion time Δ, and applied with a maximum gradient strength G. In the implemented home-built system discussed in 2.4, the maximum gradient strength G is controlled by adjusting the voltage of a controlling power supply, which precisely controls the maximum current pulsed through the gradient coil.

If T_2 is extremely short, as is the case for our solid polymers samples, the signal can become completely attenuated at time 2τ by Equation 2.12 and the diffusion coefficient cannot be measured with the spin-echo pulse sequence for any significant diffusion time Δ. Instead, a pulsed-field-gradient stimulated echo (PFGSE) [35] sequence can be used to measure diffusion

coefficients and is described in Figure 2.3. By the application of two $\pi/2$ pulses instead of the single π pulse used in the spin echo experiment, the stimulated echo sequence allows for longer diffusion times Δ by storing the nuclear spin magnetization along the z-axis (between the second pulse and third pulse), where it is subject to T_1 relaxation in contrast to faster T_2 relaxation.

In the sequence, the spins are subject to T_2 relaxation while we apply the gradient field, between the first pulse and second pulse, as well as the third pulse and fourth pulse. Therefore, for successful measurements of the solid polymer dry samples with extremely short T_2 relaxation times, the applied gradient pulses must be extremely short and intense. In our experiments, the sinusoidal shaped gradient pulse was applied for a total of 300 μs with a maximum amplitude of ~3100 G/cm, using the home-built system described in Section 2.4. In addition, an acquisition delay time TE was inserted to allow eddy currents in the probe to decay before the free induction decay (FID) signal was acquired.

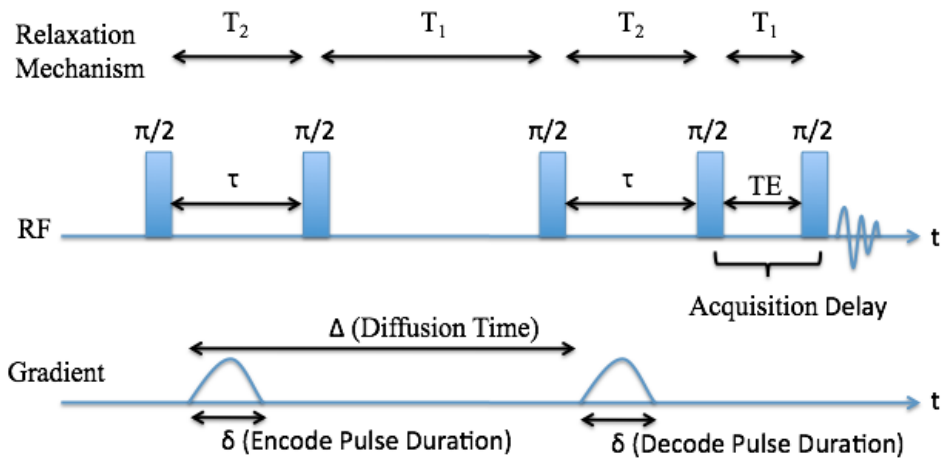

Figure 2.3: PFGSE pulse sequence diagram with important relaxation terms identified.

2.3 Gradient Coil Theory, Design, and Implementation

A gradient coil allows us to apply the spatially varying magnetic field employed in the PFGSE sequence, used to encode position of nuclei and then decode them after a diffusion time Δ. A picture of the gradient coil used in our probe and experimental set-up is shown in Figure 2.4. The coil has oppositely wound clockwise (CW) and counterclockwise (CCW) sections so that the magnetic field from the upper and lower coils oppose each other and cause a spatially varying magnetic field. The upper and lower windings sandwich the sample and RF coil aligned in the orthogonal x-y plane. The coil design is inspired by Zhang and Cory [36] and has four winding sections to implement double Maxwell Pairs for increased gradient homogeneity across the diameter of the sample [36, 37].

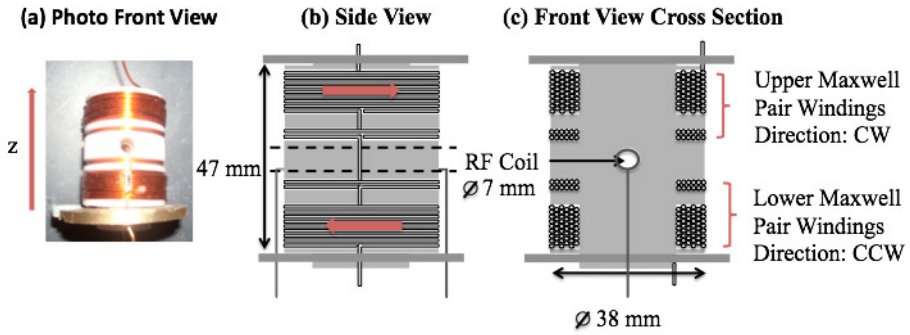

Figure 2.4: (a) A photo of the home-built gradient coil. (b) Coil Schematic Side View (c) Coil Schematic Front View Cross Section. In the upper Maxwell Pair, windings in the large and small sections were 87 and 12 respectively. In the lower Maxwell Pair, windings in the large and small sections were 80 and 11. The large winding sections were approximately ~10 windings/layer for a total of ~9 layers.

The implementation in Figure 2.4 is the second generation of a coil previously implemented and described by Tso [38]. The second generation coil was re-wound with lower gauge wire for increased gradient pulse strength and durability. Durability of the coil is a concern due to the large repeated force exerted during each gradient pulse. In particular, the coil connections and the bend points have broken several times during diffusion experiments. Each time, the coil was re-wound or repaired if possible. The final repair

included epoxy around the corners and a larger wire size to increase the coil lifetime. Because the coil was hand-wound, and due to the difficulty with maintaining tension on the wire and the bend radius of the larger wire size, the number of windings presented are approximate. The bend radius of the larger wire size was particularly problematic in keeping the number of windings per layer uniform. However, the coil has not broken despite extensive use since the described repair, so benefits of increasing wire size and using epoxy have been clearly demonstrated.

Current is pulsed through the coil in order to generate the spatially varying magnetic field using a resonance driver circuit, inspired by Conradi [39] and implemented by Tso and Michal [38]. Circuit simulations describe the charging and discharging stages of the driver circuit in Figures 2.5 and 2.6. The sinusoidal shape of the gradient pulse is measured across the 0.01 Ω shunt resistor in series with the gradient coil in the simulation. This shunt resistor is used to measure the gradient pulse using an oscilloscope. The simulation and experimental result were in very good agreement and the measured current through the gradient pulse reaches a maximum of 120 A and has a time duration of 318 μs. An important aspect of the circuit is how it allows for complete shut-off at the end of the current pulse through the gradient coil. The complete shut-off avoids unwanted interference with diffusion measurements. Modifications were made to the charge capacitor to allow for a more intense and longer gradient pulse than originally implemented by Tso and Michal [38]. The modifications were motivated by a need to measure slower diffusion coefficients in the dry polymer electrolyte material.

The initial coil used in the described experimental results was calibrated by Tso [38] using the known diffusion coefficient of water at 25°C and measuring the signal intensity of ^{1}H. The diffusion coefficient of ^{7}Li in a 1.2 M LiCl in H_2O solution at room temperature was measured with the home-built probe and a found to be 1.1x10^{-5} cm^2/s. This diffusion coefficient measurement was compared to previous measurements in the literature that were measured and plotted as a function of concentration. The previous data could be interpolated to give a value of 0.95x10^{-5} cm^2/s and was in agreement with our diffusion coefficient measurement.[40]

After coil modification, the new gradient constant was calculated by measuring the calibration sample and using the known ^{7}Li diffusion coefficient. Furthermore, the ^{7}Li diffusion coefficient in a sample of 0.81 M LiCl in water solution at room temperature was found to be 9.6x10^{-6} cm^2/s and was also in agreement with previous measurements of approximately 1.0x10^{-5} cm^2/s [40]. Based on the final calibration, the maximum gradient strength was

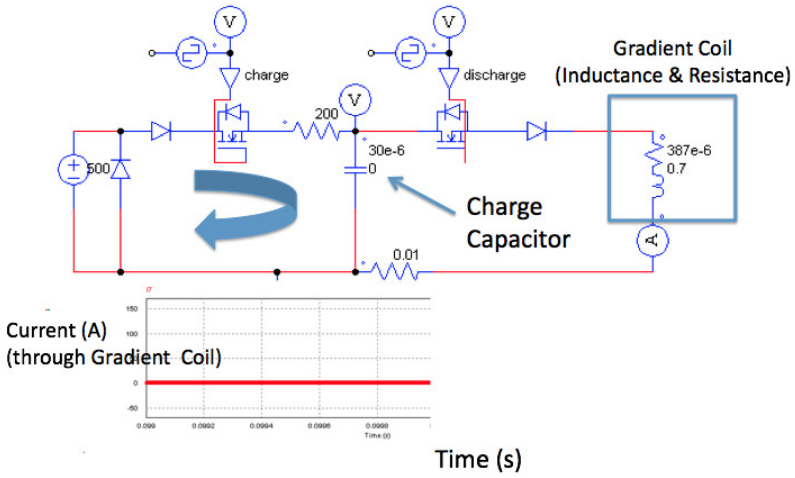

Figure 2.5: Simulation of charging stage of resonance driver circuit. A 30 μF capacitor is charged while no current flows through the gradient coil inside the probe that is schematically represented by an inductor and resistor in series.

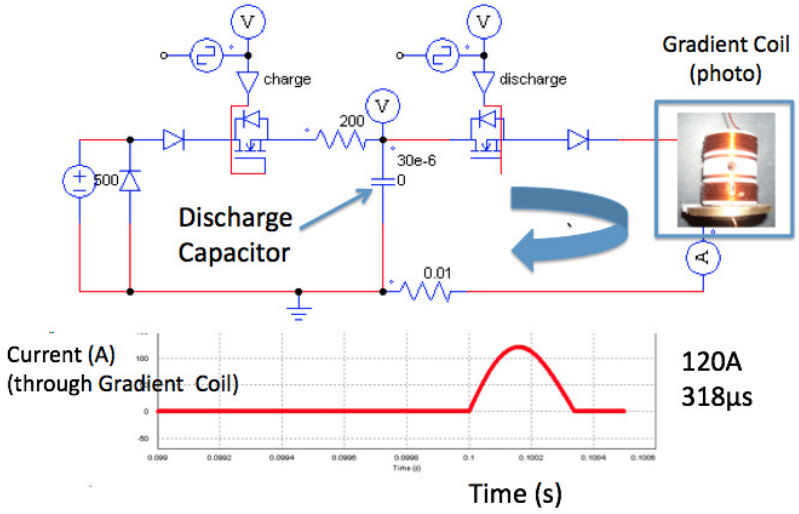

Figure 2.6: Simulation of discharging stage of resonance driver circuit. A large current of 120 A of 318 μs pulses through the gradient coil creating a short intense magnetic field pulse.

3090 G/cm.

Additionally, to confirm the gradient was behaving as expected, small amounts of current were run through the coil while observing the spectra of a 1.2 M LiCl in water solution sample. A power supply was run in a current limited state directly to the coil. NMR spectra were collected using a $\pi/2$ pulse and the width of the NMR peak in the spectrum was captured manually from each of the spectra. According to Equation 2.10, a linear scaling of the peak width was expected with increasing current through the sample. The peak width, determined at the axis (not FWHM), was observed to scale linearly with low ~mA current. The peak width scaling is demonstrated in Figure 2.7, and fit to a linear equation of y=20.6x+387. Given the small amounts of current, and that the current readings were taken directly from the power supply readout instead of using a more accurate shunt resistor, the method was meant as a qualitative check on the coil uniformity. If for example, the hand-wound coil was incorrectly wound with significantly more windings on one side than the other, it would have resulted in a spectral shift easily observed in the NMR spectra. Applying equation 2.10, and assuming the linear fit holds for significantly larger currents, and using the diameter of the sample as 0.42 cm, the result is a maximum gradient of 3500 G/cm, with 120 A flowing through the gradient coil. This value is larger than the expected 3090 G/cm but is in relative agreement. The difference is largely attributed to scaling the results of our statically applied mA currents to a dynamically pulsed maximum current of 120 A. During large pulses eddy currents are induced, that produce a field opposing the field coil. The experiment demonstrated the coil behaviour was qualitatively correct.

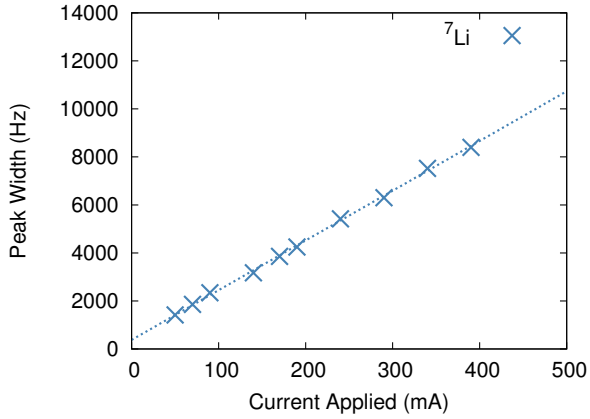

Figure 2.7: Gradient coil calibration: Increasing NMR line width with applied current to the gradient coil.

2.4 Home-built Probe Design and Implementation

In order to perform measurements with increased temperature, the home-built probe originally implemented by Tso and Michal [38] was modified. Schematics of the probe in Figures 2.8 and 2.9 identify the components added for temperature control. Room temperature air flowing up through the glass dewar was heated by a temperature controlled heating coil inside the glass dewar. At the top of the glass dewar, a custom adaptor directs the hot air flowing from the glass dewar to the sample. A thermocouple was placed inside the adaptor and just below the sample, to measure the temperature of the air heating the sample. In order to avoid heating the probe shield, an additional source of room temperature air was supplied to the area surrounding the gradient coil and sample. A small hole is visible at the top of the probe, that served as a sight hole for aligning the sample in the centre of the RF coil. A double walled vent pipe was connected to the sight hole to carry the hot air out of the spectrometer in order to avoid heat transfer to the main magnet.

A schematic of the entire system in Figure 2.10 illustrates how the temperature controller connects to the probe while inside the home-built NMR spectrometer operating at 8.4 T that is described in detail by Michal, Broughton, and Hansen.[41] The temperature set-up was calibrated with the

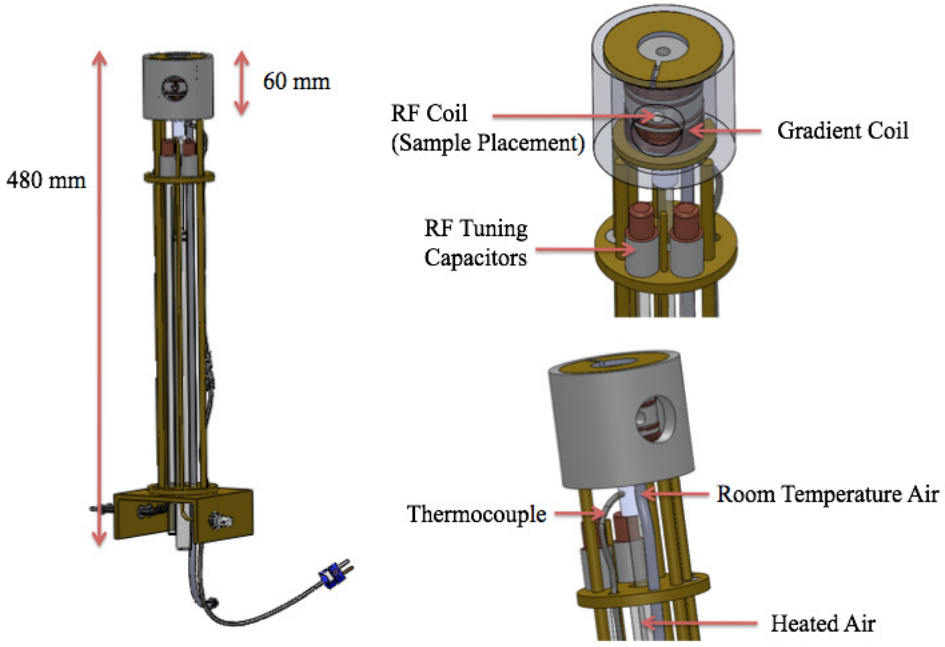

Figure 2.8: Diagram of NMR probe with temperature set-up (top view)

probe outside of the magnet. After the entire set-up was implemented, including the air vent, a second thermocouple (Mastech, MS6500) was used for calibration. At several temperature settings, an external thermocouple was touched to the sample through the sight hole from the top of the probe and the temperature of the second thermocouple was recorded. Agreement between the two thermocouples diverged at higher temperatures, as expected. A table of several calibration values is demonstrated in Table 2.1. Furthermore, the probe was left at 373 K for several hours and the temperature of the outside of the probe case was monitored to confirm the additional room temperature air supply was working to carry away hot air from the probe to avoid transferring heat to the spectrometer magnet.

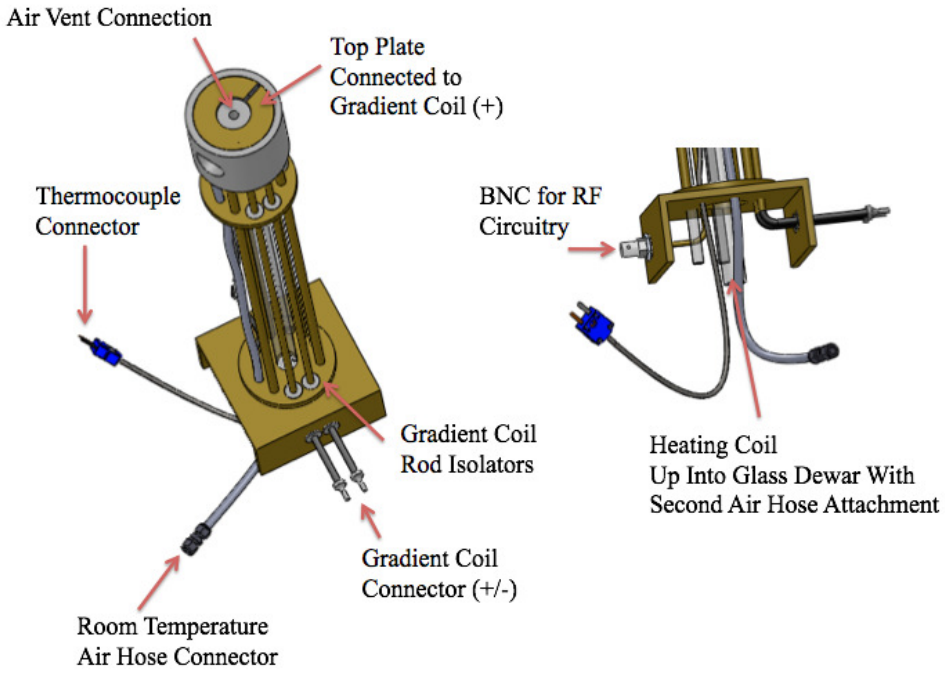

Figure 2.9: Diagram of NMR probe with temperature set-up (bottom view)

Temperature Controller Setting (K)	Sample Temperature (K)
384	373
360	353
330	328
320	319
300	301

Table 2.1: Calibration: Comparison of temperature controller temperature settings to the measured temperature at the sample with an external thermocouple.

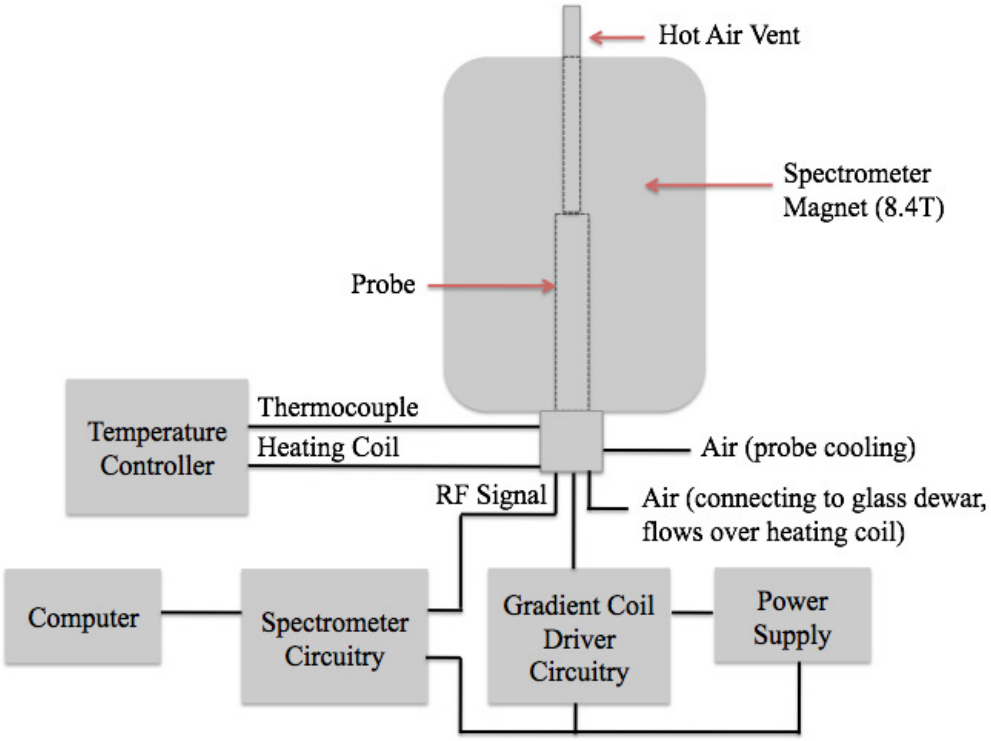

Figure 2.10: Schematic: Experimental set-up for temperature measurements.

Chapter 3

Characterization of AMLi/PEGDM Samples

The candidate solid polymer electrolyte, AMLi/PEGDM, was synthesized by our collaborators in Cergy-Pontoise University, France. The goal of the synthesis was to produce a single-ion conducting polymer. NMR characterization of the material was used to augment their initial characterization and conductivity measurements. In particular, their conductivity measurements cannot differentiate between anionic and cationic transport. Using NMR, we can confirm if their synthesis was successful in producing a single-ion conducting material.

Following a brief discussion of the materials synthesis and expected characteristics, we discuss the results of our NMR measurements. Using PFG measurements we were able to confirm the extent to which the material is single-ion conducting and fluorinated anions immobilized. Additionally, T_1 and T_2 relaxation measurements provide insight into the mobility of ions and uniformity of the polymer material. Samples were characterized in their dry and PC saturated states.

3.1 Material Overview

Our Cergy-Pontoise collaborators synthesized several samples by crosslinking an anionic monomer AMLi, illustrated in Figure 3.1, with poly(ethylene glycol) dimethacrylate (PEGDM, M=750 g/mol) by free-radical polymerization initiated with AIBN in ethanol. The AMLi lithium pair of the anionic monomer (AMLi) was synthesized using the precursor AMH, described previously.[42] Solution was poured into a mould made of two glass plates clamped together and sealed with a 100 μm thick Teflon gasket, heated, and dried under vacuum. Thin film polymer membranes with an opaque brown color were produced. The networks were abbreviated as AMLi/PEGDM X/Y, with X and Y representing the AMLi monomer and PEGDM weight proportions, respectively. The goal of the synthesis was to incorporate the

AMLi monomer into the crosslinked network so that the fluorinated anions were immobilized, producing a single-ion conducting polymer network where lithium cations can move freely and fluorinated anions were immobilized as part of a crosslinked polymer network. It was thought that ionic motion occurred by intra- and inter-chain hopping in the crosslinked polymer matrix. Ionic conductivity σ_{EXP} of the AMLi materials was measured by AC impedance spectroscopy (VSP, Bio-logic) in the frequency range from 1 MHz to 1 Hz with an oscillation potential of 10 mV. The polymer film was sandwiched between two stainless steel electrodes, and measurements were performed under argon atmosphere up to 393 K. Conductivities of the dry material were ~3.0x10^{-7} S/cm and ~1.0x10^{-4} S/cm in propylene carbonate (PC) saturated samples at 30°C .

NMR relaxation and diffusion measurements were performed on the AMLi/PEGDM X/Y samples in a dry state at temperatures up to 373 K. Additionally, PC was added to dry samples in order to characterize the samples in their gel state. PC saturated samples demonstrated higher conductivity and would also exhibit single-ion conducting properties if the synthesis technique was successful.

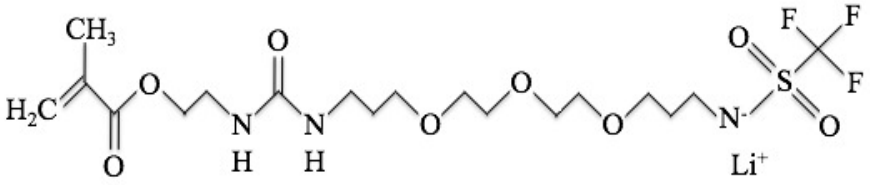

Figure 3.1: AMLi monomer structure

3.2 Dry Sample Measurements

3.2.1 Line Width and Relaxation Measurements

At room temperature, the ^{7}Li and ^{19}F spectra of the AMLi/PEGDM 40/60 sample were observed. On initial qualitative inspection, the ^{7}Li spectra appeared to have two components, with a narrow Lorentzian peak superposed on a broad Gaussian component. The FWHM of the broad and narrow components were approximately 4.5 kHz and 1 kHz respectively. In contrast, the ^{19}F spectra appeared as a single peak, with FWHM approximately 1.8

kHz. The ^{19}F and ^{7}Li spectra were acquired with 8 and 16 acquisitions respectively and are demonstrated in Figure 3.2. The two component nature of the ^{7}Li spectra indicated the presence of two distinct local environments.

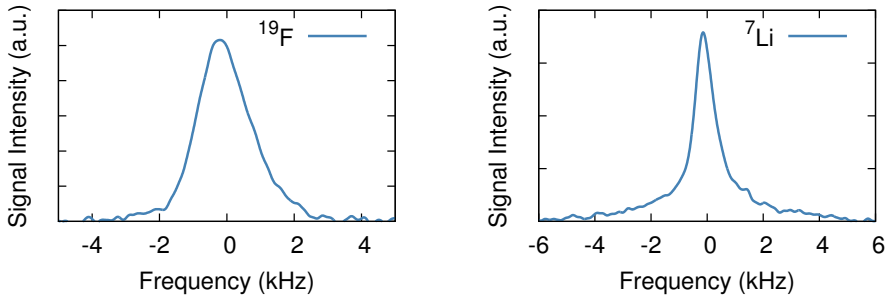

(a) ^{19}F (b) ^{7}Li

Figure 3.2: AMLi/PEGDM 40/60 dry sample ^{19}F and ^{7}Li spectra.

To characterize the short range motions of the lithium cations in the dry AMLi/ PEGDM 40/60 sample through the glass transition T_g of -26°C, T_1 relaxation inversion recovery experiments (ie. π-τ-$\frac{\pi}{2}$-Acq.) were performed. The line widths (ideally inversely proportional to T_2 relaxation) were also observed. For below room temperature measurements, experiments were performed at 9.4 T on a Varian Unity Inova 400 MHz NMR spectrometer using a Varian/Chemagnetics wideline double resonance Apex probe with a 5 mm diameter coil. The above room temperature measurements were performed using the 8.4 T 363 MHz home-built spectrometer and probe described in Section 2.4. The relaxation time approaches a minimum above the transition temperature and rises sharply at lower temperatures as observed in Figure 3.3. Although there is a slight difference in resonant frequencies between the two spectrometers (141 MHz and 155 MHz), the results were comparable. The transition from longer to shorter T_1 times is reflective of glassy and rubbery materials properties below and above the glass transition, characteristic of a crosslinked polymer material.[43] Although one would expect two T_1 relaxation components corresponding to the narrow and broad peaks, a single T_1 relaxation time has been used. Based on a previous study by Adamic and Greenbaum[24], we expect the two T_1 times are relatively close together at higher temperatures but become increasingly different at lower temperatures. At room temperature, the two T_1 times were different by a factor of two and the rest of the data appears to be consistent with

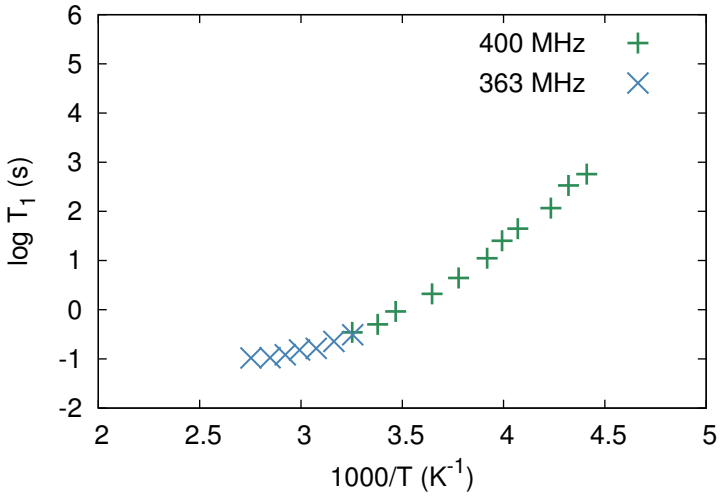

Figure 3.3: Inversion Recovery T_1 relaxation measurements of a dry AMLi/PEGDM 40/60 sample. The single-component relaxation time approaches a minimum above the glass transition temperature Tg 1000/T = 4.0 K^{-1} (-26°C) and rises sharply at lower temperatures.

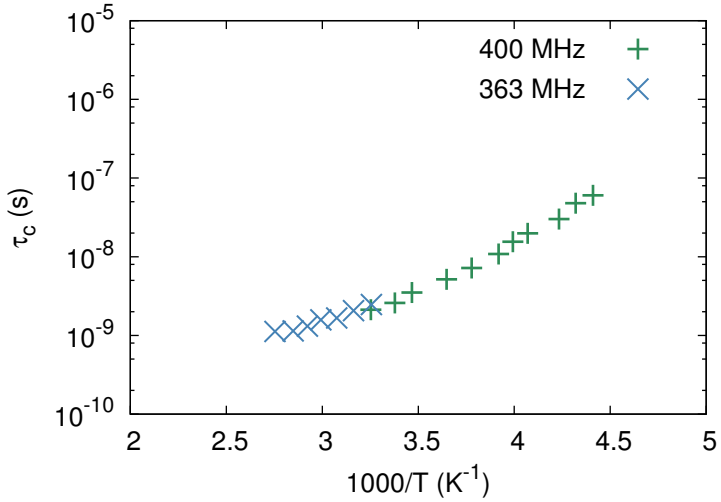

Figure 3.4: Lower limit of correlation times, calculated from the T_1 relaxation measurements in Figure 3.3 of the dry AMLi/PEGDM 40/60 sample.

our expectations. However, the quality of the data and low signal to noise did not justify two-component fits and therefore a single exponential fit was used.

We can approximate the correlation times in order to compare our measurements to the literature. In the extreme narrowing condition where $\omega\tau_c \ll 1$ the T_1 of the ^{7}Li (I=3/2) undergoing isotropic reorientation is given by [18, 20]

$$\frac{1}{T_1} = \frac{\omega_q^2}{50}\left(\frac{\tau_c}{1+\omega_o^2\tau^2} + \frac{4\tau_c}{1+4\omega_o^2\tau_c^2}\right), \tag{3.1}$$

where τ_c is the correlation time introduced in Figure 1.5, ω_q is the quadrupolar coupling constant, and ω_o is the resonant frequency (rad/s). As the sample is close to the T_1 minimum where $\omega_o\tau_c = 1$, far away from the solid regime of Figure 1.5, we will approximate correlation times using Equation 3.1 although the sample is not actually in the extreme narrowing condition where $\omega\tau_c \ll 1$.

According to this method, if we take an assumption the sample is near the T_1 minimum at a temperature of 363 K, we can calculate the lower limit of the correlation times. Using Hayamizu's approach [18], we have calculated the quadrupolar coupling constant ω_q from the value of τ_c at the minimum corresponding to $1 = \omega_o\tau_c$. Using the T_1 minimum of 375 ms, ω_q is approximated as 3.0x10^5 rad/s. The resulting lower limits of the correlation times at each temperature are demonstrated in Figure 3.4. They are longer than the correlation times calculated for ^{7}Li by Hayamizu in room temperature ionic liquids, as expected. At a temperature of 2.8 (1000/T K^{-1}), the lower limit of our correlation times are ~10^{-9} s compared with the ionic liquids with correlation times in the range of 10^{-10} to 10^{-9} s.

At higher temperatures, the spectra associated with the single T_1 relaxation times had a narrow peak superposed on a broad peak as demonstrated in Figure 3.5. The line width (FWHM) of the narrow and broad component were approximately 1 kHz and 5 kHz at 35°C. At lower temperatures, the broad and narrow components were indistinguishable and the single peak had a line width (FWHM) of approximately 7 kHz at -46°C. Interestingly, the broad contribution was evident above the glass transition temperature. Therefore, the lithium cations were located in two distinct environments even above the glass transition, with the narrow component characteristic of a more mobile environment and the broad component characteristic of a less mobile environment. Motional narrowing observed in the central peak reflects mobility due to polymer segmental motion necessary for ionic

conductivity.[23–25, 43] The described spectra were consistent with Adamic and Greenbaum's observations[24] in their study of MEEP/PEO/$LiClO_4$ polymer electrolyte films. However, the broad line width was much narrower than observed by Panero et al[23].

To investigate the two-component nature at more elevated temperatures, much greater than T_g, transverse relaxation T_2 measurements using a Hahn spin-echo pulse sequence (ie.$\frac{\pi}{2}$-τ-π-τ-Acq.) were performed up to 100°C (NMR spectral line widths are inversely proportional to T_2 relaxation times in the absence of inhomogeneous broadening). At more elevated temperatures, T_2 relaxation times were two-component, however the broad component became less distinguishable. The single peak had a FWHM line width of approximately 0.8 kHz at 100°C. The relaxation results are summarized in Table 3.1 and the reduction of the broad component at elevated temperatures is reflected in the increase in the T_2 times. At room temperature, approximately 70% of the ^{7}Li measured was associated with the shorter T_2 time and less mobile broad component. At 100°C the less mobile component was reduced to less than 60% and the T_2 time corresponds to a much narrower line width. The relaxation data analyzed to produce these results have poor signal to noise due to a grounding issue (later resolved) and a low number of acquisitions. However, the qualitative results capture the disappearance of the broad component at elevated temperatures and a decrease in the amount of the low mobility component with temperature. A gradual reduction in the low mobility component of this AMLi/PEGDM 40/60 dry sample is consistent with the gradual increase in conductivity experimentally observed in each of the AMLi/PEGDM X/Y dry samples.

Temperature (°C)	T_{2a} (ms)	T_{2b}(ms)	a/b
22	0.088	1.1	0.73/0.27
61	0.466	13.0	0.73/0.27
78	0.419	11.5	0.59/0.41
100	0.541	10.8	0.56/0.44

Table 3.1: Multi-component ^{7}Li transverse relaxation times for a dry AMLi/PEGDM 40/60 sample. Two components, T_{2_a} and T_{2_b} were observed up to 100°C in an abundance of a and b expressed as a fraction of the total.

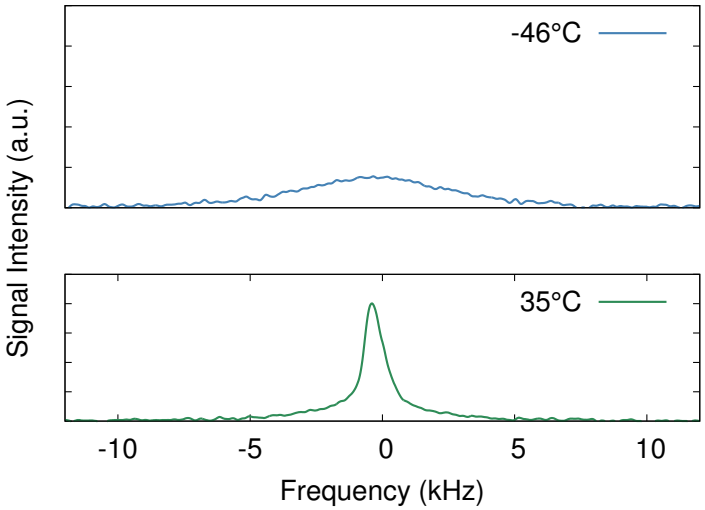

Figure 3.5: AMLi/PEGDM 40/60 spectra at -46°C and 35°C measured using a Varian Unity Inova 400 MHz NMR spectrometer. At elevated temperatures, a narrow central peak superposed on a broad Gaussian peak was observed. Well below room temperature and T_g a single broad peak was observed.

3.2.2 Diffusion Measurements

At elevated temperatures, diffusion in the dry samples could be observed using the PFGSE pulse sequence. Unexpectedly, diffusion of fluorinated anions, in addition to lithium cations, was observed (by signal attenuation in the PFGSE experiment). The ^{19}F and ^{7}Li diffusion coefficients of the dry sample AMLi/PEGDM 40/60 were measured at 100°C by fitting the PFGSE signal attenuation, in Figure 3.6. The diffusion coefficients were fit according to Equations 2.13 and 2.14 with the condition that the diffusion time is much greater than the time of the applied gradient pulses so $\Delta \gg \delta$. Therefore the signal attenuation was fit according to

$$S(x) = Ae^{-4\Delta D(\frac{\gamma \delta G_x}{\pi})^2}, \tag{3.2}$$

where the pulses are applied for a duration of δ, separated by a diffusion time Δ, and applied with a maximum gradient strength G. The cationic and anionic diffusion coefficients measured were 3.4x10^{-8} cm^2/s and 2.2x10^{-8} cm^2/s, confirming both lithium cations and fluorinated anions were mobile in the sample. As the coefficients were on the same order, the results suggested correlated motion, consistent with observations by Williamson et al[22].

Using the Nernst-Einstein Equation 1.6 gave an approximate conductivity σ_{NMR} of 1.5 x10^{-4} S/cm in contrast to the experimentally observed conductivity σ_{EXP} of 1.0 x10^{-5} S/cm at 373 K in the same sample type. As discussed in section 1.3, from the ratio $\sigma_{EXP}/\sigma_{NMR}$ we could approximate a dissociation of ~6%. This comparison supported the hypothesis of correlated diffusion. Diffusion was not observed in dry samples at room temperature, although the experimental limit was on the order of 1x10^{-9} cm^2/s and it is possible diffusion was present with a slower rate. The overestimation of conductivity using the Nernst-Einstein relation is consistent with previous studies by Arumugam et al [21] and Williamson et al [22]. They have also observed σ_{NMR} to overestimate conductivity by up to an order of magnitude.

The NMR relaxation and diffusion experimental results for the dry AMLi /PEGDM 40/60 sample were inconsistent with the expected crosslinked single-ion conducting polymer sample as both ^{7}Li and ^{19}F were able to diffuse in the sample. Furthermore, the ^{7}Li was located in two distinct local environments, even above T$_g$.

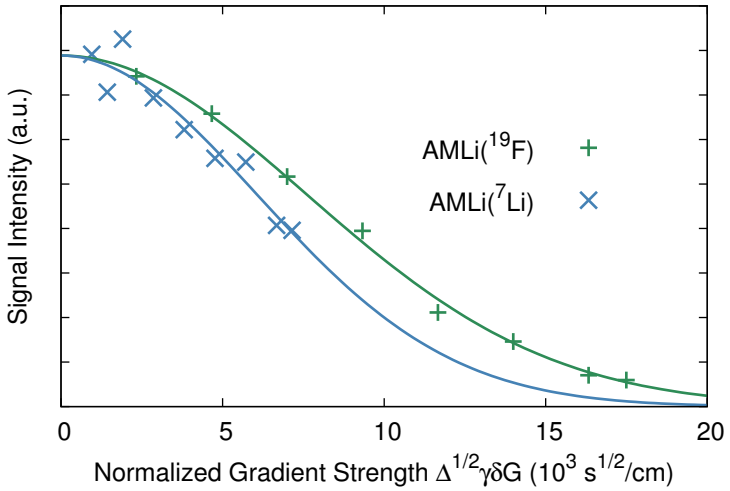

Figure 3.6: ^{7}Li and ^{19}F PFGSE data and diffusion coefficient fits for AMLi/PEGDM 40/60 at 100°C with a diffusion time Δ of 0.5 s. The x-axis is normalized for the diffusion time Δ, gradient pulse duration δ, and gyromagnetic ratio γ. Both of the data sets were captured up to the same maximum gradient pulse strength. Due to the lower γ of ^{7}Li, its data on the normalized axis ends before that of ^{19}F.

3.3 PC Saturated Samples

3.3.1 Line Width and Relaxation Measurements

Further characterization of the samples in their PC saturated state was carried out in order to gain further insight into the polymer structure. In the PC saturated state, it was expected that the ^{7}Li would have higher mobility and faster diffusion accompanied by sharper spectral lines.

Multi-component behaviour with a sharp Lorentzian peak superposed on a broad Gaussian peak was also observed in the ^{7}Li spectra of the saturated samples. At room temperature, the ^{7}Li and ^{19}F spectra of the AMLi/PEGDM 70/30 saturated sample is demonstrated in Figure 3.7. The broad and narrow components of the ^{7}Li spectra are approximately 2.5 kHz and 0.30 kHz (FWHM), less than half of the widths seen in the dry AMLi/PEGDM 40/60 of Figure 3.2. The narrow component line width was comparable to the 0.30 kHz line width observed by Croce et al[25] in a gel electrolyte above 300 K. The ^{19}F single peak has a width of approximately 0.5 kHz compared with 1.8 kHz in the dry AMLi/PEGDM 40/60 sample. In the figure, the ^{19}F spectra was taken with 64 acquisitions while the ^{7}Li spectra was taken with 16 acquisitions.

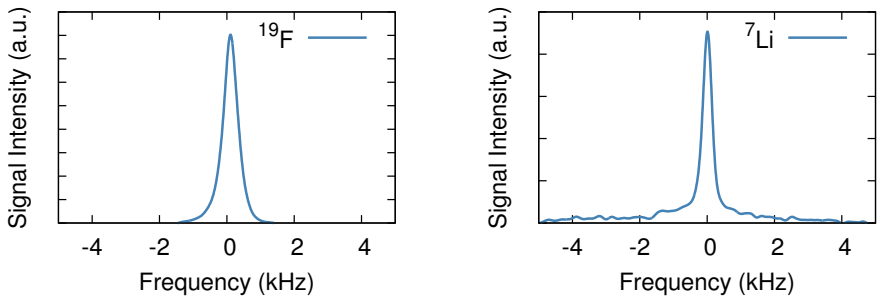

(a) ^{19}F (b) ^{7}Li

Figure 3.7: AMLi/PEGDM 70/30 PC saturated sample ^{19}F and ^{7}Li spectra.

Relaxation measurements were performed to characterize the ^{7}Li mobility in each of the two local environments. Inversion recovery data were fit with two components according to

$$f(T_{1_{ab}}) = a(1 - 2e^{-\tau_R/T_{1_a}}) + b(1 - 2e^{-\tau_R/T_{1_b}}) + z, \tag{3.3}$$

and the spin echo data were fit according to

$$f(T_{2_{abc}}) = ae^{(-2\tau_E/T_{2_a})} + be^{(-2\tau_E/T_{2_b})} + ce^{(-2\tau_E/T_{2_c})}, \tag{3.4}$$

where the coefficients a, b, and c, correspond to the relative abundance of each of the relaxation components T_{1_a},T_{1_b} and T_{2_a},T_{2_b}, and T_{2_c}. The multi-component exponential fit results are demonstrated in Figure 3.8 for the case of AMLi/PEGDM 70/30. Notice the curves do not exhibit single exponential behaviour.

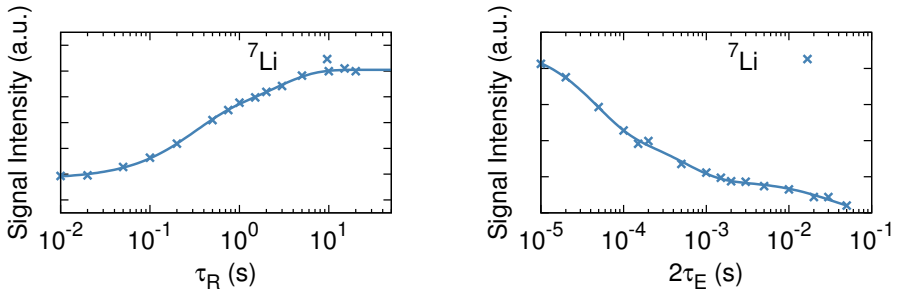

(a) T_1 (b) T_2

Figure 3.8: Multi-component relaxation measurements of PC saturated AMLi/PEGDM 70/30. T_{1_a}/T_{1_b} were 2567/273 ms in a ratio a/b of 0.44/0.56. $T_{2_a}/T_{2_b}/T_{2_c}$ were 0.089/1.08/67.2 ms in a ratio a/b/c of 0.51/0.30/0.19.

In order to support our multi-component exponential fits, and to confirm if there were two or three components in each of the measurements, the spectra of each of the individual data points in the inversion recovery and spin echo experiments were analyzed. For example, the spectra of the recovery times τ_R of 10 ms, 100 ms, 200 ms, and 5000 ms were analyzed. The spectra at each of these points are captured in Figure 3.9. The line shape clearly exhibited multi-component behaviour as it crossed the horizontal axis at τ_R of 200 ms with a slowly relaxing broad Gaussian component and fast relaxing sharper Lorentzian. To numerically confirm our relaxation results, each of the spectra was individually fit with a Lorentzian and Gaussian according to

$$f(x) = \frac{a}{\pi}\left(\frac{\tau/2}{(x-x_o)^2 + (\tau/2)^2}\right) + \frac{j}{\sqrt{2\pi\sigma^2}}e^{-(x-\mu)^2/2\sigma^2} + z\,, \tag{3.5}$$

with the Lorentzian and Gaussian corresponding to the fast and slow components respectively. The signal intensities of each of the individual Lorentzian and Gaussian fits are demonstrated in Figure 3.10. The Gaussian portion was fit to a single exponential while the Lorentzian portion was fit with a double exponential. Finally, all of the relaxation results found by equations 3.3 and 3.4 compared with the method of individually fitting the spectra by equation 3.5 are in Table 3.2. The agreement between the two methods support the multi-component exponential fit to the integrated signal intensities. Thus, it was concluded the more simple multi-exponential fit to integrated signal intensities could be applied to these samples to accurately capture the multi-component relaxation times.

As in the case of the dry sample relaxation measurements, the single broad Gaussian component was characteristic of ^{7}Li in a less mobile environment and unaveraged dipolar or quadrupolar couplings. These interactions have a strong spatial dependence and were attributed to an immobile ^{7}Li component. The sharper Lorentzian components are attributed to two distinct local environments of mobile ^{7}Li ionic species contributing toward conductivity.

Relaxation Times	Relaxation Fit Results (ms)	Spectral Fit Results (ms)
T_{1a} (Gaussian)	2567	2000
T_{1b} (Lorentzian)	273	295
a/b	0.44/0.56	0.55/0.45
T_{2a} (Gaussian)	0.089	0.073
T_{2b} (Lorentzian)	1.08	0.80
T_{2c} (Lorentzian)	67.2	79.3
a/b/c	0.51/0.30/0.19	0.39/0.33/0.28

Table 3.2: Multi-component ^{7}Li relaxation times for a PC saturated AMLi/PEGDM 70/30 sample, with abundance a, b, and c, expressed as a fraction of the total. A comparison of relaxation times found by multi-exponential fits of integrated signal intensities of the spectra versus individual fits to each of the spectra is presented. The relaxation times found from each of the methods were in agreement, supporting the multi-component fit results.

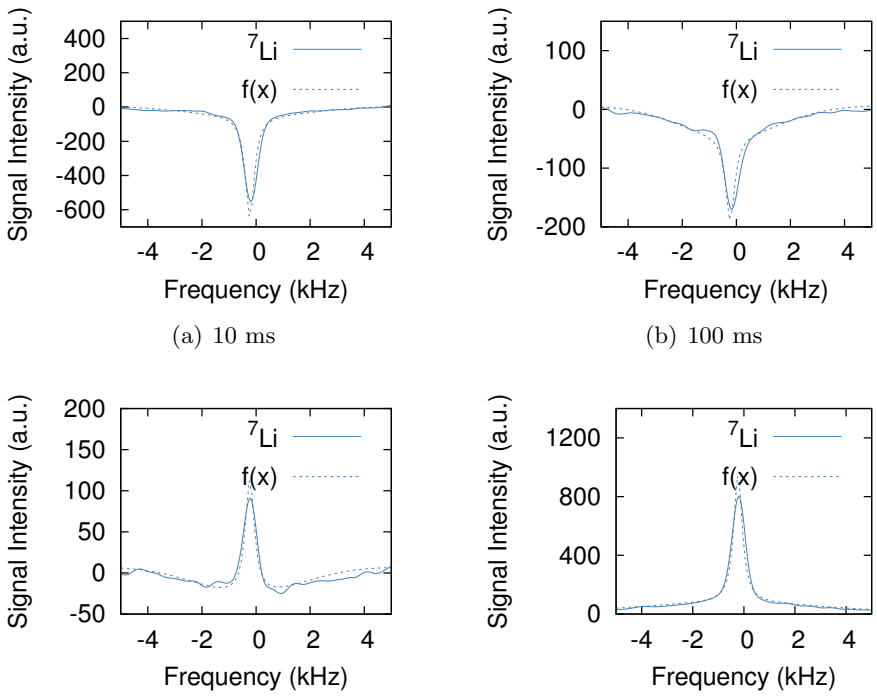

(a) 10 ms

(b) 100 ms

(c) 200 ms

(d) 5000 ms

Figure 3.9: ^{7}Li spectra of PC saturated AMLi/PEGDM 70/30 from an inversion recovery experiment at 10 ms, 100 ms, 200 ms and 5000 ms. A data fit according to Equation 3.5 is overlaid on the data. Notice the two component behaviour of the spectra, with a fast relaxing Lorentzian and slowly relaxing Gaussian.

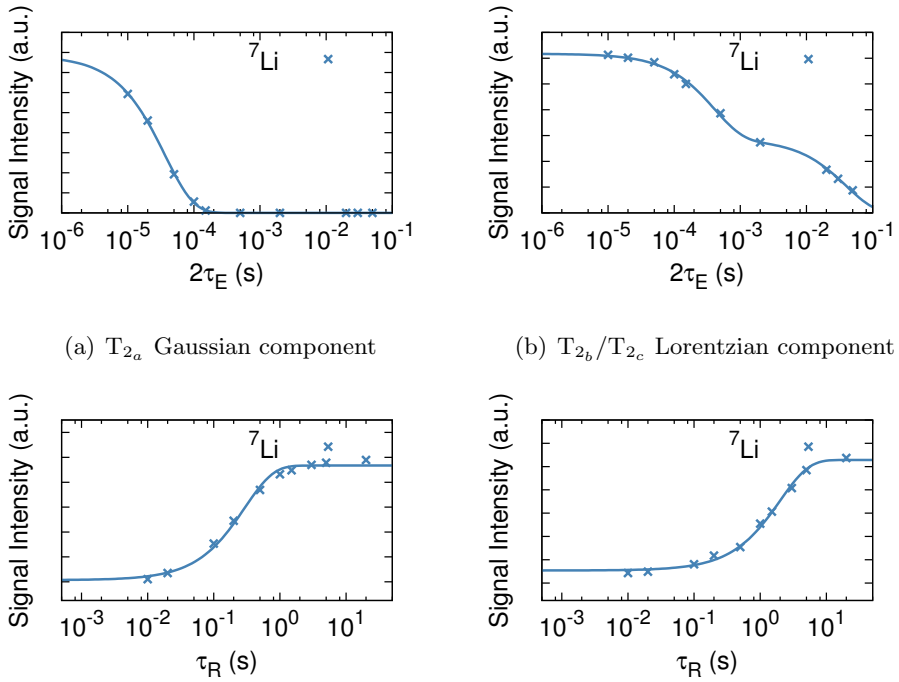

(a) T_{2_a} Gaussian component

(b) T_{2_b}/T_{2_c} Lorentzian component

(c) T_{1_a} Gaussian component

(d) T_{1_b} Lorentzian component

Figure 3.10: Multi-component relaxation fits of PC saturated AMLi/PEGDM 70/30 obtained by analyzing the Lorentzian and Gaussian components separately. The values of the coefficients of the Lorentzian and Gaussian components resulting from the fits to each spectrum were plotted against the inversion recovery time τ_R and twice the spin echo time $2\tau_E$. (a) The T_{2_a} component results from fitting the component to $a\exp(-2\tau_E/T_{2_a})$ (b) The T_{2_b} and T_{2_c} components result from fitting the Lorentzian component to $b\exp(-2\tau_E/T_{2_b}) + c\exp(-2\tau_E/T_{2_c})$ (c) The T_{1_a} component results from fitting the component to $a(1-2\exp(-\tau_R/T_{1_a})) + z$ (d) The T_{1_b} component results from fitting the component to $b(1-2\exp(-\tau_R/T_{1_b})) + z$.

3.3.2 Diffusion Measurements

In addition to relaxation measurements, PFGSE diffusion measurements were performed on AMLi/PEGDM X/Y samples saturated with PC. Results are demonstrated for PC saturated AMLi/PEGDM 70/30 in Figure 3.11 and the diffusion coefficients are summarized in Table 3.3. In Figure 3.11, the two-component ^{19}F diffusion data were fit according to

$$S(x) = Ae^{-4\Delta D_{A-}(\frac{\gamma\delta G_x}{\pi})^2} + Be^{-4\Delta D_{B-}(\frac{\gamma\delta G_x}{\pi})^2} + z, \tag{3.6}$$

and the ^{7}Li data were fit according to

$$S(x) = Ae^{-4\Delta D_{+}(\frac{\gamma\delta G_x}{\pi})^2} + z. \tag{3.7}$$

The two-component anion diffusion suggests some immobilization of the fluorine, with the first component diffusing an order of magnitude slower than the second component. The second fluorinated anionic diffusion coefficient (^{19}F D_{B-}) is of similar magnitude to the lithium diffusion coefficient (^{7}Li D_{+}), suggesting correlated diffusion. Thus, the fluorinated anions were not completely immobilized in a crosslinked network. The presence of additional ^{19}F and ^{7}Li diffusion coefficients arising from components with short T_1 (<200 ms) and/or T_2 times (<0.5 ms) cannot be ruled out, as they would be strongly suppressed in the PFGSE diffusion experiment. Furthermore, not all of the lithium and fluorine is mobile in the sample, evident from the constant offset z in the equation fits 3.6 and 3.7. In particular, a large fraction of the observable ^{7}Li signal did not diffuse appreciably on the timescale observed, evident in Figure 3.11. The z values, representing the fraction of the signal that did not display any appreciable diffusion during the time Δ of the experiments, are included in Table 3.3.

3.4 Additional AMLi/PEGDM samples

We have discussed the relaxation measurements of dry AMLi/PEGDM 40/60 and saturated AMLi/PEGDM 70/30 as well as some diffusion measurement results of PC saturated AMLi/PEGDM 50/50, 70/30, and 80/20. In addition to the results presented, further ^{7}Li and ^{19}F relaxation and diffusion measurements were performed on dry and PC saturated samples. As the results were consistent with the results already presented, they are not included in this thesis in detail. However, we will briefly mention some trends and similarities between the samples for the reader.

X/Y Samples	^{7}Li D_{+} (cm^2/s)	Ratio (A/z)	^{19}F D_{A-}/D_{B-} (cm^2/s)	Ratio (A/B/z)
50/50	$9.8x10^{-7}$	0.23/0.77	$3.0x10^{-7}/1.7x10^{-6}$	0.73/0.24/0.03
70/30	$1.3x10^{-6}$	0.70/0.30	$4.5x10^{-7}/3.1x10^{-6}$	0.58/0.40/0.02
80/20	$1.0x10^{-6}$	0.58/0.42	$3.1x10^{-7}/2.2x10^{-6}$	0.51/0.47/0.02

Table 3.3: Summary of diffusion coefficients measured in PC saturated AMLi/PEGDM X/Y samples. Diffusion times Δ were 350 ms and 500 ms for ^{7}Li and ^{19}F measurements. Abundance ratios are expressed as a fraction of the total. They are not quantitative because they are severely weighted by relaxation effects.

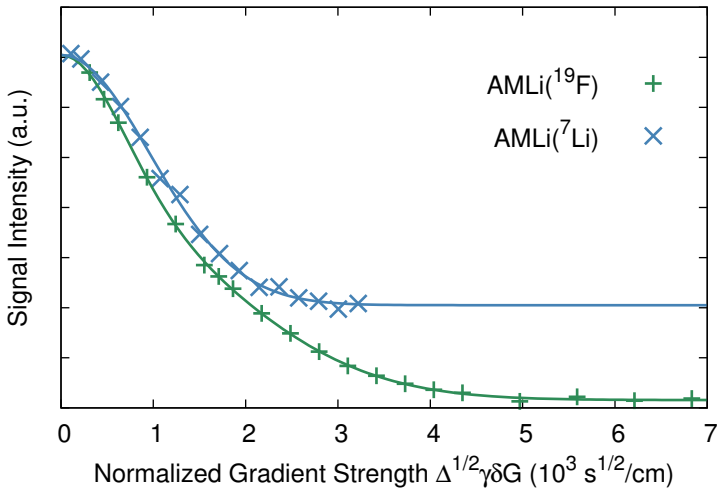

Figure 3.11: ^{7}Li and ^{19}F PFGSE data and diffusion coefficient fits for PC saturated AMLi/PEGDM 70/30 at room temperature with ^{7}Li and ^{19}F diffusion times of 0.35 s and 0.5 s. The x-axis is normalized for the diffusion time Δ, gradient pulse duration δ, and gyromagnetic ratio γ. Both of the data sets were captured up to the same maximum gradient pulse strength. Due to the lower γ of ^{7}Li, its data on the normalized axis ends before that of ^{19}F.

The multi-component relaxation behaviour was consistent across all of the sample variants in dry and PC saturated states. Consistent with the ^{7}Li AMLi/PEGDM 40/60 relaxation results presented, dry AMLi/PEGDM 70/30 and 80/20 samples also exhibited two-component T_1 and T_2 relaxation behaviour. The ^{19}F relaxation measurements were single component in all of the dry samples. Consistent with the PC saturated AMLi/PEGDM 70/30 ^{7}Li relaxation results presented, the saturated 50/50 and 80/20 samples also exhibited multi-component behaviour. The slowly relaxing Gaussian and fast relaxing Lorentzian components were also clearly visible in the ^{7}Li spectra of the 50/50 and 80/20 PC saturated samples. For the case of ^{19}F, single-component T_1 relaxation and multi-component T_2 relaxation was observed in the 50/50, 70/30, and 80/20 saturated samples. The 40/60 sample was not measured in the PC saturated state but would be expected to exhibit similar relaxation behaviour.

Neither ^{7}Li nor ^{19}F diffusion coefficients were measurable in any of the dry samples at room temperature. As the stronger gradient coil and temperature apparatus was not implemented while the 50/50, 70/30, and 80/20 samples were in their dry state, diffusion was only observed in the dry 40/60 sample at elevated temperatures.

Chapter 4

Characterization of AMLi/PEGDM w/DCPD Sample

Based on the two-component nature of the diffusion results in the saturated samples (Table 3.3), it was hypothesized that leftover uncrosslinked monomer from the synthesis could be contributing to the results. New samples were extracted in ethanol. Analysis of the obtained product indicated the presence of side reactions appearing during the polymerization in ethanol that could prevent the formation of fully crosslinked material. For subsequent samples the synthesis was modified, using THF instead of ethanol. After optimization, DiCyclohexyl PeroxydiCarbonate (DCPD) was added as a replacement for AIBN. The new AMLi/PEGDM w/DCPD samples with lower content of AMLi showed negligible extractable component.

The goal of the synthesis was to produce a single-ion conducting polymer as with the original AMLi/PEGDM samples of Chapter 3. Therefore, it was expected that the cationic diffusion coefficient would be much greater than that of the anionic diffusion coefficient as the fluorine would be immobilized in the crosslinked network and no extractable component remained in the thin-film polymer samples.

4.1 Line Width and Relaxation Measurements

First, we will discuss observations of the AMLi 20/80 w/DCPD samples and compare them to the dry AMLi/PEGDM 40/60 dry samples. The ^{7}Li spectra has a central peak width of 0.7 kHz (FWHM) compared to the AMLi/PEGDM 40/60 dry sample of 1 kHz. There was a broad component of approximately 2.2 kHz (FWHM) compared with that of AMLi/PEGDM 40/60 of 4.5 kHz. These narrower widths indicate more motional averaging in this sample compared to AMLi/PEGDM 40/60, suggesting increased lithium cation mobility. The ^{19}F spectra was a single broad peak, with a

width of approximately 1.8 kHz (FWHM) that was approximately the same as that of AMLi/PEGDM 40/60. The ^{7}Li spectrum in Figure 4.1 was taken with 64 acquisitions and the ^{19}F spectra with 16 acquisitions. For a similar sample size (~1/2), the ^{7}Li signal intensity was approximately 1/10 of the AMLi/PEGDM 40/60, noticeably smaller. However, the ^{19}F signal intensity was approximately double. These results suggest that in the process of removing extractable components, the amounts of ^{7}Li and ^{19}F in the sample were altered compared to previous samples.

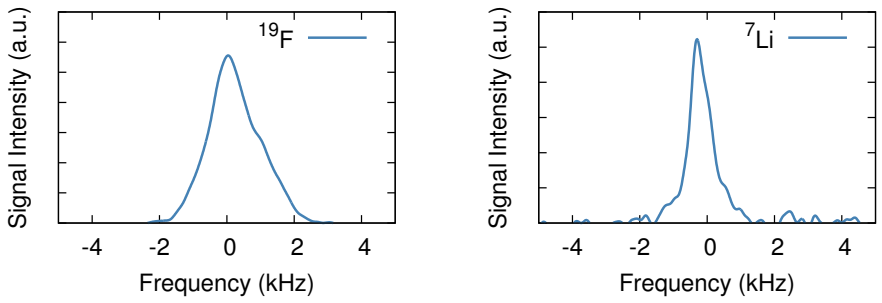

(a) ^{19}F (b) ^{7}Li

Figure 4.1: AMLi/PEGDM 20/80 w/DCPD dry sample ^{19}F and ^{7}Li spectra.

Relaxation measurements were performed in order to characterize the sample. ^{7}Li and ^{19}F experimental results are demonstrated in Figures 4.2 and 4.3. The two-component T_2 relaxation results indicate lithium ions are in two local environments associated with lower and higher mobility, consistent with the observations of the spectra in Figure 4.1. Approximately 70% of the lithium ions were associated with the lower mobility component. The ^{19}F nuclei were also located in two distinct local environments with relative proportions matching those of the ^{7}Li nuclei. Interestingly, there were two ^{19}F T_1 relaxation components while a single component adequately described the ^{7}Li T_1 relaxation. The T_2 relaxation components were consistent with the AMLi/PEGDM 40/60 sample of Section 3.2.1. However, the second component of the AMLi/PEGDM 40/60 sample was less mobile and further to the right in the solid regime of Figure 1.5.

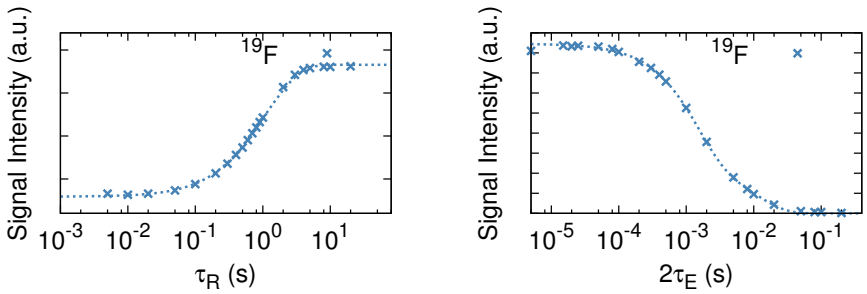

(a) T_1 Relaxation (b) T_2 Relaxation

Figure 4.2: ^{19}F inversion recovery and spin echo relaxation measurements of dry AMLi/PEGDM w/DCPD sample at 373 K. Integrated signal intensity is plotted against relaxation time τ_R and twice the echo time τ_E. (a) T_{1_a}/T_{1_b} are 1432/437 ms fit by $f(\tau_R) = a(1 - 2\exp(-\tau_R/T_{1a})) + b(1 - 2\exp(-\tau_R/T_{1b})) + z$ and (b) T_{2_a}/T_{2_b} are 2.87/22.1 ms fit by $f(\tau_E) = a\exp(-2\tau_E/T_{2a}) + b\exp(-2\tau_E/T_{2b})$.

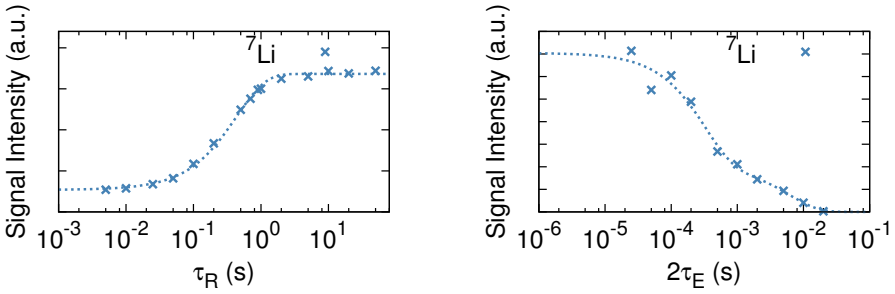

(a) T_1 Relaxation (b) T_2 Relaxation

Figure 4.3: ^{7}Li inversion recovery and spin echo relaxation measurements of dry AMLi/PEGDM w/DCPD sample at 373 K. Integrated signal intensity is plotted against relaxation time τ_R and twice the echo time τ_E. (a) T_{1_a} is 435 ms fit by $f(\tau_R) = a(1 - 2\exp(-\tau_R/T_{1a})) + z$ and (b) T_{2_a}/T_{2_b} are 0.645/12.3 ms fit by $f(\tau_E) = a\exp(-2\tau_E/T_{2a}) + b\exp(-2\tau_E/T_{2b})$.

4.2 Diffusion Measurements

Next, ^{7}Li and ^{19}F diffusion coefficients were measured, and again showed correlated motion between the cationic and anionic nuclear species. The PFG diffusion measurements are demonstrated in Figure 4.4. The two-component ^{19}F diffusion data were fit according to

$$S(x) = Ae^{-4\Delta D_{A-}(\frac{\gamma\delta G_x}{\pi})^2} + Be^{-4\Delta D_{B-}(\frac{\gamma\delta G_x}{\pi})^2}, \tag{4.1}$$

and the ^{7}Li data were fit according to

$$S(x) = Ae^{-4\Delta D_{+}(\frac{\gamma\delta G_x}{\pi})^2}. \tag{4.2}$$

Two anionic diffusion coefficients of 2.4x10^{-8} cm^2/s and 1.9x10^{-9} cm^2/s were observed, thus the fluorine was not completely immobilized. The cationic diffusion coefficient of 2.0x10^{-8} cm^2/s was obtained from a single exponential data fit, although a second component may have also been present and not observed due to signal attenuation of the component with the shorter T_2 time.

4.3 Quantification of Diffusing Species

4.3.1 Method and Calibration

As fluorinated anions were unexpectedly mobile in our AMLi samples, experiments were performed to address the question of how much of the fluorine was contributing toward diffusion and therefore unsuccessfully incorporated into the crosslinked network. To accomplish this, relaxation times causing exponential signal intensity decay during the PFGSE experiment were accounted for and a calibration sample was used with a known number of ions. By accounting for relaxation, we were able to extrapolate our results backwards to find the total amount of each diffusing component. These quantities could be directly compared to relaxation results and we were able to quantify the number of ions diffusing of each of the fluorinated anionic components to gain insight into how much of the fluorine was successfully immobilized.

From Figure 2.3, we can see the important relaxation terms identified in the PFGSE pulse sequence. It follows the final signal intensity has the form

$$S(x) = A(N)\, e^{\left(\frac{-2\tau}{T_2}\right)} e^{\left(\frac{-(\Delta-\tau)}{T_1}\right)} e^{\left(\frac{-TE}{T_1}\right)} e^{\left(-D(4\Delta-\delta)\left(\frac{\gamma\delta G_x}{\pi}\right)^2\right)}, \tag{4.3}$$

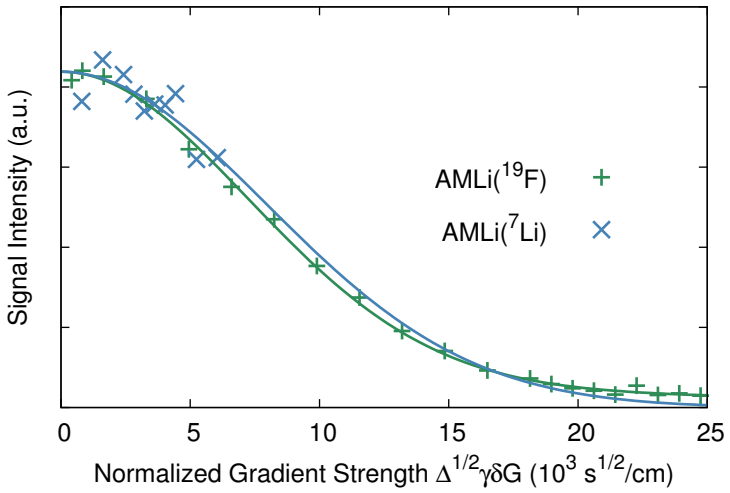

Figure 4.4: ^{7}Li and ^{19}F PFGSE data and diffusion coefficient fits for AMLi/PEGDM 20/80 w/DCPD sample at 373 K with a ^{19}F and ^{7}Li diffusion time Δ of 1000 ms and 350 ms. The x-axis is normalized for the diffusion time Δ, gradient pulse duration δ, and gyromagnetic ratio γ. Both of the data sets were captured up to the same maximum gradient pulse strength. Due to the lower γ of ^{7}Li, its data on the normalized axis ends before that of ^{19}F.

and in the case of two-component relaxation and diffusion times, the two components were handled separately, with coefficients corresponding to the amount of each component diffusing:

$$S(x) = A(N_a)\, e^{\left(\frac{-2\tau}{T_{2_a}}\right)} e^{\left(\frac{-(\Delta-\tau)-TE}{T_{1_a}}\right)} e^{\left(-D_a(4\Delta-\delta)\left(\frac{\gamma\delta G_x}{\pi}\right)^2\right)} + A(N_b)\, e^{\left(\frac{-2\tau}{T_{2_b}}\right)} e^{\left(\frac{-(\Delta-\tau)-TE}{T_{1_b}}\right)} e^{\left(-D_b(4\Delta-\delta)\left(\frac{\gamma\delta G_x}{\pi}\right)^2\right)}. \quad (4.4)$$

The coefficient term $A(N)$ depends on the number of ions, N. Also in the coefficient term is a calibration factor β, the number of acquisitions in the experiment N_{acq}, and finally a factor of 1/2 resulting from the stimulated echo pulse sequence. For Li^+, the expression for the coefficient in our samples is

$$A(N) = \frac{\beta N_{Li} N_{acq}}{2}, \quad (4.5)$$

and in the case where we have more than one detected nucleus per molecule, a factor corresponding to the number of nuclei per molecule is included. For example, in the case we are interested in a salt with 6 F per molecule, a factor of 6 is added:

$$A(N_{F_6}) = \frac{\beta 6 N_{F_6} N_{acq}}{2}. \quad (4.6)$$

In order to find the calibration factor, β, samples of known weight and composition were measured for ^{19}F and ^{7}Li probe tuning calibrations. 1.1 M TBAP (tetrabutylammonium hexafluorophosphate) in PC (propylene carbonate) and 0.81 M LiCl in water solutions were used. A small spherical sample was accurately centred in the RF coil. T_1 and T_2 relaxation times were measured in the context of the PFGSE pulse sequence by varying the parameters τ and Δ. In addition, more standard diffusion PFGSE measurements, where the gradient strength was increased as a function of voltage of the controlling power supply unit, were performed. Including the known number of ions, N, all of the data was simultaneously fit according to Equation 4.3 varying parameters T_1, T_2, D, and the calibration factor β. In cases where runaway parameter fits occurred, the set of fit variables was restricted. In order to confirm the final fit values, the relaxation times and diffusion coefficients D determined by this method were compared with more standard inversion recovery and spin echo relaxation measurements.

For a ^{19}F probe tuning calibration using TBAP/PC solution, the data obtained by varying the two time parameters and pulsed gradient strength in three separate experiments, and the simultaneous data fit is demonstrated in Figure 4.5. Note the time parameters measured were relevant to experiments

on the sample of interest, AMLi/PEGM 20/80 w/DCPD, and therefore did not capture the entire relaxation decay of the calibration samples. From the set of experiments and fit to Equation 4.3, a calibration factor β of 5.69x10^7 integrated signal intensity per mol was found. A new calibration constant was found from a full set of PFGSE and relaxation measurements each time the probe was changed between ^{19}F and ^{7}Li tuning.

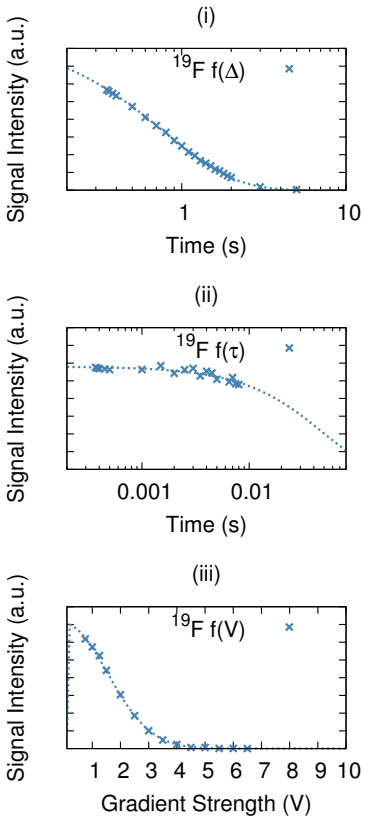

Figure 4.5: ^{19}F PFGSE measurements of a 1.1M TBAP/PC calibration sample at room temperature (i) T_1 measurement by varying parameter Δ (ii) T_2 measurement by varying parameter τ and (iii) Diffusion coefficient measurement by varying the gradient strength as a function of voltage V. Using the known number of ions in the sample, all of the data was simultaneously fit in order to determine a calibration constant β.

4.3.2 PEGM/PEGDM/LiTFSI Reference Samples

In order to validate the technique, reference samples of PEGM/PEGDM/ LiTFSI (Bis(trifluoromethane)sulfonimide lithium salt M=287 g/mol) were measured, where the fluorinated anions and lithium cations could move freely and were expected in a 1:1 ratio. The samples were also prepared by our Cergy-Pontoise collaborators, as in section 3.1. Dry samples of PEGM/PEGDM/LiTFSI and PC saturated samples contained a weight percentage of 11% and 6% of LiTFSI respectively. The amounts of LiTFSI were therefore 4.0x10^{-5} mols and 4.4x10^{-5} mols in the dry and PC saturated samples. The structure of LiTFSI is shown in Figure 4.6. It has a single lithium nucleus and 6 fluorine nuclei per molecule therefore we are comparing quantities of 1 Li to 6 F, or N_{Li} to N_{F_6}.

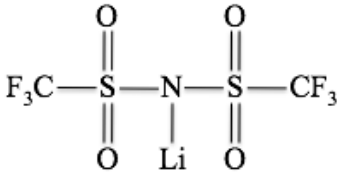

Figure 4.6: Structure of LiTFSI

As the samples were quite large and difficult to centre in the tube, a significant portion of the samples protruded outside of the RF coil. This impacted the absolute quantification measurements because the signal contribution from the sample outside of the coil was less than if it was in the centre of the RF coil. A correction factor was obtained by preparing the calibration samples with a comparable size to that of the PEGM/PEGDM/LiTFSI samples, and comparing signal intensities between the larger samples and the original small spherical samples that were accurately centred in the centre of the RF coil. The signal correction factor obtained was 5x and was applied to the final total quantities. More important than the quantitative accuracy of these measurements was the relative quantities of the N_{Li} and N_{F_6}, which do not depend on this correction factor.

A dry sample of PEGM/PEGDM/LiTFSI was first characterized by T_1 and T_2 relaxation measurements. The relaxation results and curve fits for ^{7}Li and ^{19}F are demonstrated in Figures 4.7 and 4.8.

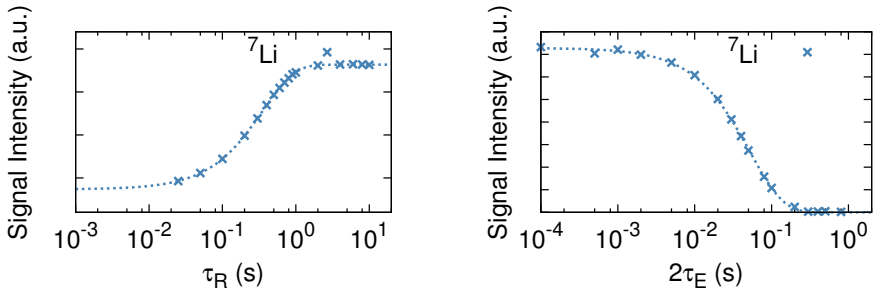

(a) T_1 Relaxation (b) T_2 Relaxation

Figure 4.7: ^{7}Li inversion recovery and spin echo relaxation measurements of dry PEGM/PEGDM/LiTFSI samples at 373 K. Integrated signal intensity is plotted against relaxation time τ_R and twice the echo time τ_E (a) T_1 is 356 ms fit by $f(\tau_R) = a - 2b\exp(-\tau_R/T_1)$ and (b) T_2 is 105 ms fit by $f(\tau_E) = a\exp(-2\tau_E/T_2)$.

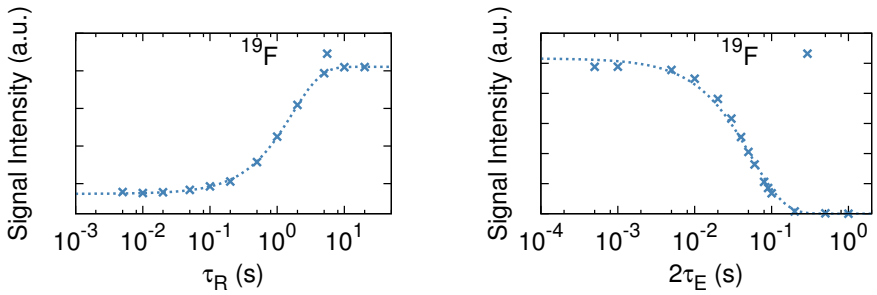

(a) T_1 Relaxation (b) T_2 Relaxation

Figure 4.8: ^{19}F inversion recovery and spin echo relaxation measurements of dry PEGM/PEGDM/LiTFSI at 373 K. Integrated signal intensity is plotted against relaxation time τ_R and twice the echo time τ_E. (a) T_1 is 1686 ms fit by $f(\tau_R) = a - 2b\exp(-\tau_R/T_1)$ and (b) T_2 is 109 ms fit by $f(\tau_E) = a\exp(-2\tau_E/T_2)$.

The relaxation values were single component, consistent with a homogeneous sample. In contrast to the AMLi/PEGDM X/Y samples, all of the ^{7}Li is mobile, with T_1 and T_2 times of 356 ms and 105 ms approximately equal, characteristic of a small molecule in a non-viscous liquid, and consistent with the mid-left region of Figure 1.5.[17] The larger relative difference between the ^{19}F T_1 and T_2 relaxation times of 1686 ms and 109 ms are characteristic of a larger molecule, tumbling more slowly, also consistent with the expected result in the right region of Figure 1.5. In contrast to the AMLi/PGDM X/Y samples of Chapter 3, there was no second broad Gaussian component indicating a semi-solid phase.

Next, a set of PFGSE experiments were performed. The numbers of ions diffusing, N, relaxation values T_1 and T_2, and diffusion coefficient D were obtained, using the ^{7}Li and ^{19}F calibration values of β. The observed data and equation fits for ^{7}Li and ^{19}F measurements are demonstrated in Figure 4.9. The comparison of the relaxation results using the two experimental methods are compared in Table 4.1.

Relaxation Times	Relaxation Measurements		PFGSE Measurements	
	^{7}Li	^{19}F	^{7}Li	^{19}F
T_1 (ms)	356	1686	373	1626
T_2 (ms)	105	109	68	35

Table 4.1: Comparison of ^{7}Li and ^{19}F PEGM/PEGDM/LiTFSI dry sample relaxation results at 373 K from inversion recovery and spin echo relaxation measurements versus PFGSE measurements.

The T_1 relaxation values for ^{7}Li and ^{19}F were found to be 373 ms and 1626 ms in the PFGSE experiment, versus 356 ms and 1686 ms using the inversion recovery and spin echo measurements of Figures 4.7 and 4.8. The T_2 relaxation values were both reduced by a factor of ~1.5 and ~3 in the PFGSE experimental fit for ^{7}Li and ^{19}F in Figure 4.9 compared to the more standard inversion recovery and spin echo relaxation measurements. Although in relative agreement, these values were thought to be reduced by eddy currents in the gradient coil. The gradient pulse was always applied at the start of the T_2 delay time (τ in Figure 2.3) in the PFGSE sequence and therefore eddy currents would cause additional dephasing to the magnetization in the x-y plane.

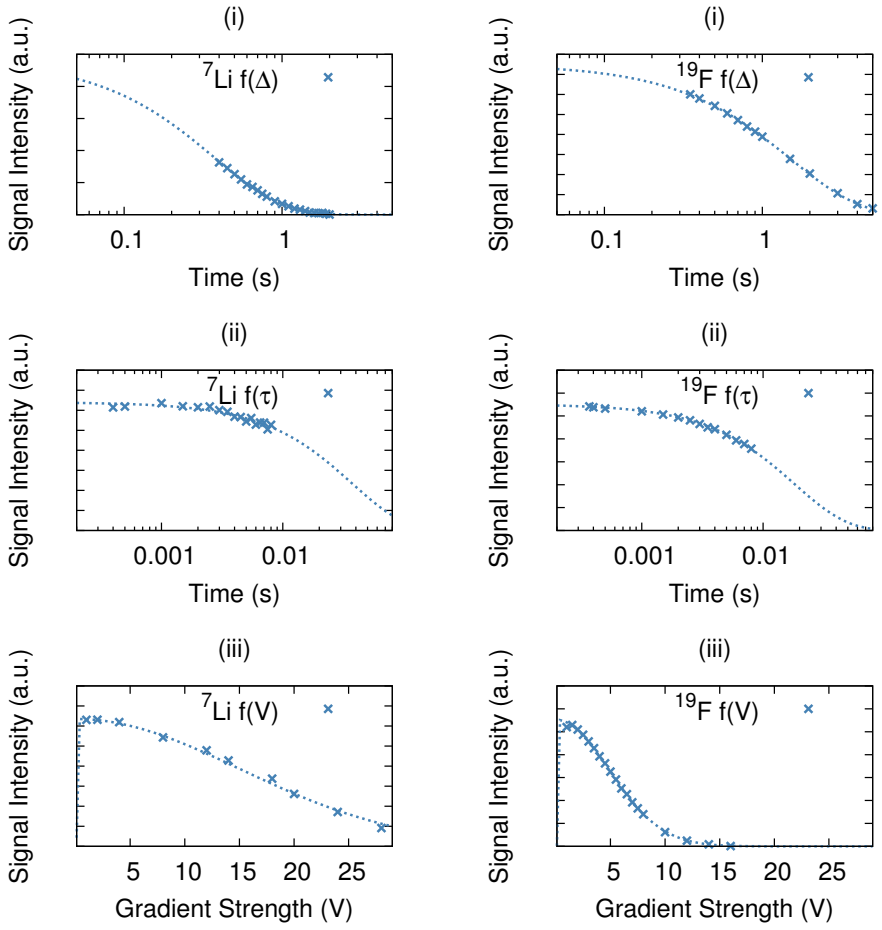

(a) ^{7}Li PFGSE Experiments (b) ^{19}F PFGSE Experiments

Figure 4.9: ^{7}Li and ^{19}F PFGSE measurements of a dry PEGM/PEGDM/ LiTFSI sample at 373 K. For each nuclear species there are a set of three experiments (i) T_1 measurement by varying parameter Δ (ii) T_2 measurement by varying parameter τ and (iii) Diffusion coefficient measurement by varying the gradient strength as a function of voltage V.

Also from the equation fits of Figure 4.9, the quantity of ions diffusing, N, were found to be 7.1x10^{-5} mols of lithium cations (1 nucleus/salt molecule) and 5.8x10^{-5} mols of fluorinated anions (6 nuclei/salt molecule) in a ratio of approximately 1:1, as expected. The quantity results for the dry sample, as well as the saturated sample, are summarized in Table 4.2.

PEGM/PEGDM/LiTFSI Samples	N_{Li} (mols)	N_{F_6} (mols)	$N_{Li} : N_{F_6}$
Dry Sample at 373K	7.1x10^{-5}	5.8x10^{-5}	0.55:0.45
PC Saturated Sample at 298K	8.2x10^{-5}	7.1x10^{-5}	0.54:0.46

Table 4.2: Quantities of lithium cations and fluorinated anions diffusing in dry and PC saturated PEGM/PEGDM/ LiTFSI samples at 373 K and 298 K. The amount of Li and F_6 are expressed as a fraction of the total.

The total number of lithium cations and fluorinated ions were in qualitative agreement with the expected numbers of 4.0x10^{-5} mols (dry) and 4.4x10^{-5} mols (w/PC), based on the samples' compositions. The measured numbers of ions diffusing in these samples included a correction factor to account for the fact that a significant fraction of the sample protruded outside of the NMR coil. Uncertainty in the correction factor likely accounts for the remaining discrepancy (x1.5) between the measured and expected values. Future work would incorporate more uniform sample sizes for increased accuracy, although the overall agreement was satisfactory and the consistency between the results found with the two different nuclear species inspires confidence in the technique.

4.3.3 AMLi/PEGDM 20/80 w/DCPD Sample

After validating the quantification technique with the (LiTFSI) reference samples, it was applied to our AMLi/PEGDM 20/80 w/DCPD dry sample at 373 K. In this case, the results would quantify multiple components. The goal was to investigate how many of the fluorinated anions were contributing to the diffusion results and the extent to which they were successfully immobilized in the polymer network.

Next, ^{19}F and ^{7}Li PFGSE experiments were performed. The ^{19}F PFGSE data and equation fits are shown in Figure 4.10. Because of the extremely low signal strength of ^{7}Li, significant time was required to perform these measurements. 2048 acquisitions were taken over several days for each of

the PFGSE experiments compared to the ^{19}F measurements where only 64 acquisitions were taken for each experiment for adequate signal to noise ratio. Although several weeks of experiments were performed using the PFGSE method, results were inadequate to gain confident insight into the behaviour of each of the T_2 components and to accurately quantify the amount of ^{7}Li diffusing. This was attributed to a short T_2 component and low signal intensity. However, the total number of ions diffusing was estimated from relaxation measurements. The relaxation times found for each of the described methods are compared, in addition to the relative abundance of each component (a and b), in Table 4.3.

Relaxation Times	Relaxation Measurements ^{7}Li	Relaxation Measurements ^{19}F	PFGSE Measurements ^{7}Li	PFGSE Measurements ^{19}F
T_{1_a}/T_{1_b} (ms)	435	1432/437	-	1401/464
Quantities (a/b)		0.77/ 0.23		0.72/0.28
T_{2_a}/T_{2_b} (ms)	0.645/12.3	2.87/22.1	-	2.66/33.5
Quantities (a/b)	0.71/0.29	0.71/0.29		0.72/0.28

Table 4.3: Comparison of ^{7}Li and ^{19}F AMLi/PEGDM 20/80 w/DCPD dry sample inversion recovery and spin echo relaxation results versus PFGSE results at 373 K.

In the case of standard diffusion measurements, the relative abundance was found from the coefficient belonging to each component in the inversion recovery and spin echo fits in Figure 4.2 and 4.3 and in the case of PFGSE experiments, the relative abundance is found from the number of ions found to be diffusing of each component N_a and N_b. For the fluorinated anions, the relative abundance of each component found in the PFGSE method was in agreement with the corresponding relaxation measurements, supporting the equation fit of the PFGSE experiments.

Results of quantities of ions diffusing of each component are summarized in Table 4.4. The total amount of ^{7}Li diffusing was estimated from inversion recovery and spin echo signal intensities, however the amount of individual components diffusing is not included for reasons described above. The measured quantities of fluorinated and lithium ions diffusing were unexpected as they were not in equal ratios. The amount of AMLi monomer expected based on weight and composition was $5.8\text{x}10^{-6}$ mols. However, the

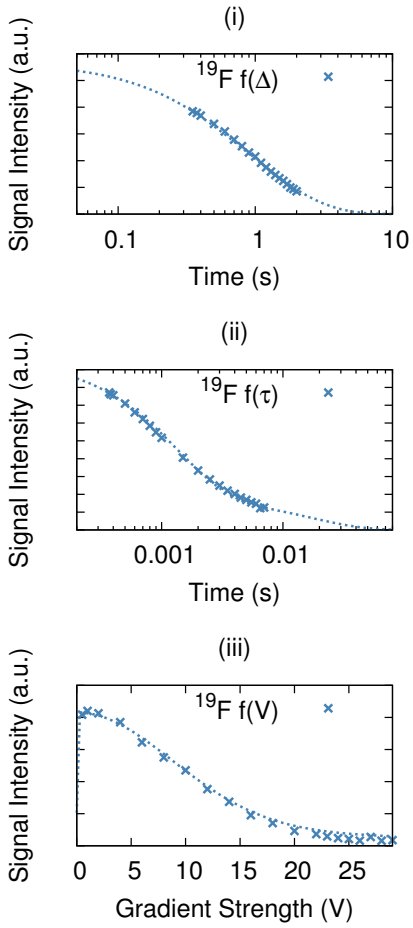

Figure 4.10: ^{19}F PFGSE measurements of a dry AMLi/PEGDM 20/80 w/DCPD sample at 373 K. A set of three experiments (i) T_1 measurement by varying parameter Δ (ii) T_2 measurement by varying parameter τ and (iii) Diffusion coefficient measurement by varying the gradient strength as a function of voltage V.

quantification experiments found roughly four times more ^{19}F but only half the ^{7}Li expected. Furthermore, in contrast to the PEGM/PEGDM/LiTFSI samples in section 4.3.2, this sample was more contained inside the RF coil and the measured quantities were expected to agree more closely with the expected quantities. As our experimental technique has been validated with the (LiTFSI) reference samples, these results reflect some unknown result of the synthesis method. The results also provided a quantitative explanation why the ^{7}Li experiments were so challenging. Furthermore, our results demonstrate that all of the fluorine is mobile in the sample.

	Component		
	a		b
$^{7}Li\,D_{+}\,(cm^2/s)$	2.0x10^{-8}		-
$^{19}F\,D_{-}\,(cm^2/s)$	2.4x10^{-8}		1.9x10^{-9}
N_{Li} (mols)		2x10^{-6}	
N_{F_3} (mols)	1.5x10^{-5}		6.1x10^{-6}
N_{F_3} (a/b)	0.72		0.28
Ratio N_{F_3}/N_{Li}		10.7	

Table 4.4: Summary of dry AMLi/PEGDM 20/80 w/DCPD diffusion coefficients measured at 373K. Allowed diffusion times Δ of $^{7}Li\,D_{+}$ and $^{19}F\,D_{-}$ were 350 ms and 1000 ms respectively. The relative abundance of N_{F_3} components a and b are expressed as a fraction of the total. The total quantities of N_{F_3} and N_{Li} are expressed as a ratio.

The two-component behaviour of the ^{19}F diffusion measurements was in agreement with the corresponding relaxation measurements. The first anionic component had an almost identical diffusion coefficient to that of ^{7}Li of ~2x10^{-8} cm^2/s, suggesting highly correlated diffusion. The second anionic diffusion coefficient of 1.9x10^{-9} cm^2/s is an order of magnitude less, suggesting this component is less mobile in the polymer network. A corresponding component for ^{7}Li was not observed but may be present with a T_2 time too short or diffusion coefficient too low to be observed. Quantitative ^{7}Li measurements of the sample in the PC saturated state agreed with the dry state measurements, with the diffusion coefficient 1.75x larger, 3.5x10^{-8} cm^2/s.

The relaxation and diffusion measurement results are inconsistent with a single-ion conducting crosslinked polymer. The fluorine was mobile and correlated with lithium diffusion. The relaxation results indicated both lithium and fluorine were located in two distinct local environments with lower and higher mobility. The quantities associated with the two ^{19}F diffusion coefficients were in agreement with the relaxation measurements. Thus, the lower and higher mobility components could be attributed to each diffusion coefficient. Quantitative comparison of the conductivities between σ_{NMR} and σ_{exp} are not possible as the σ_{exp} was not measured on the same sample at the same temperature of 373 K. As a qualitative comparison, comparable dry samples of AMLi/ PEGDM 40/60 and AMLi/PEGDM 50/50 had a measured conductivity of ~1x10^{-5} S/cm compared with conductivity estimated from the NMR measurements σ_{NMR} of 1.0 x10^{-4} S/cm at 100°C. Comparing these conductivities suggests a dissociation of ~10%. Further work is therefore required to fully immobilize the fluorinated anions in a crosslinked network.

Chapter 5

Characterization of PEO/PEO-b-PE/$LiClO_4$ Samples

A second candidate solid polymer electrolyte incorporating poly(ethylene oxide)-block-polyethylene (PEO-b-PE) is under investigation in Zhong's research group at Washington State University. The polymer electrolytes are not intended to be single-ion conducting and both the cations and anions are mobile in the samples. Therefore, it is expected to have a low transference number. Work has already been completed characterizing its structure, electrical conductivity, and mechanical properties.[11, 44, 45] The aim of their synthesis is to improve conductivity and mechanical properties simultaneously.

A series of copolymer samples contain a conductive block (PEO block) and a reinforcement block (PE block).[11] Materials used were poly(ethylene oxide) (MW = 4x10^6 g/mol), poly(ethylene oxide)-block-polyethylene (PEO-b-PE) (875 with 80 wt% PE, 920 with 50 wt% PE), and lithium perchlorate ($LiClO_4$) obtained from Aldrich.[11] The polymer films were prepared by dissolving PEO, $LiClO_4$, and the copolymer in acetonitrile. The polymer films were formed on a glass substrate and left at room temperature until the solvent was evaporated.[11, 44] Three samples, PEO/$LiClO_4$, PEO/PEO-b(920)-PE/$LiClO_4$, and PEO/ PEO-b(875)-PE/$LiClO_4$ were prepared.

An increase of conductivity (using AC measurements) and enhanced mechanical properties compared to PEO electrolytes has been demonstrated. Conductivities of the (875) and (920) samples were reported as 3.2x10^{-4} S/cm and 1.1x10^{-5} S/cm at room temperature.[11] The glass transition temperatures reported were approximately -62°C (875) and -59°C (920).[11] We have analyzed the three samples using ^{7}Li PFG NMR over a temperature range up to 66°C to augment the characterization already completed.

5.1 Line Width and Relaxation Measurements

The ^{7}Li spectra of the PEO/PEO-b(920)-PE/$LiClO_4$ is demonstrated in Figure 5.1. The spectrum was taken with only 4 acquisitions as the signal intensity was much stronger compared to the AMLi/PEGDM 40/60 samples, approximately 10x. The width of the peak (FWHM) was approximately 0.6 kHz, that was approximately equal to the central peak widths of the AMLi/PEGDM w/DCPD (0.7 kHz) and PC saturated AMLi/PEGDM 40/60 (0.5 kHz) samples. Compared to the AMLi/PEGDM 40/60 sample that had a broad Gaussian component of 4.5 kHz, no broad Gaussian component was evident.

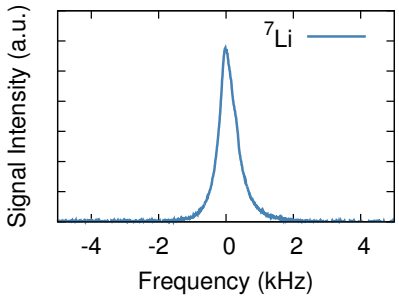

(a) ^{7}Li

Figure 5.1: PEO/PEO-b(920)-PE/$LiClO_4$ dry sample ^{7}Li spectra.

Relaxation measurements were completed for each of the three samples. All of the T_1 relaxation data was adequately described by a single exponential. The T_2 relaxation data required a double exponential fit, and was therefore two-component. The two-component data indicated the presence of two local environments. The relaxation data is summarized in Table 5.1. The majority of the ^{7}Li was in the less mobile environment (~65%) associated with the shorter T_2 time. The relative difference of the T_1 and T_2 times are consistent with the mid-region of Figure 1.5, as expected for ^{7}Li mobility in a polymer electrolyte.

	$PEO/LiClO_4$	(875)	(920)
T_{1a} (ms)	279	316	312
T_{2a} (ms)	3.28	0.99	2.16
T_{2b} (ms)	35.1	28.4	25.3
a/b	0.65/0.35	0.67/0.33	0.64/0.36

Table 5.1: ^{7}Li relaxation times for the $PEO/LiClO_4$, and PEO/PEO-b-$PE/LiClO_4$ (875) and (920) samples, with abundance a and b expressed as a fraction of the total.

5.2 Diffusion Measurements

The diffusion coefficient measurements are demonstrated in Figures 5.2, 5.3 and 5.4 and the diffusion coefficients are summarized in Table 5.2. In the case of PEO/$LiClO_4$, the diffusion coefficient increased by a factor ~16 from 22° to 60°C. Similarly, the PEO/PEO-b(920)-PE/$LiClO_4$ and PEO/PEO-b(875)-PE/$LiClO_4$ increased by factors of 15 and 13.

Sample	^{7}Li Self Diffusion Coefficients D (cm^2/s) 22°C	45°C	60°C
PEO/$LiClO_4$	5.12x10^{-9}	2.18x10^{-8}	8.31x10^{-8}
PEO/PEO-b(920)-PE/$LiClO_4$	3.02x10^{-9}	2.31x10^{-8}	4.56x10^{-8}
PEO/PEO-b(875)-PE/$LiClO_4$	3.39x10^{-9}	1.68x10^{-8}	4.36x10^{-8}

Table 5.2: Summary of NMR diffusion coefficients of dry PEO/PEO-b-PE/$LiClO_4$ samples up to 60°C.

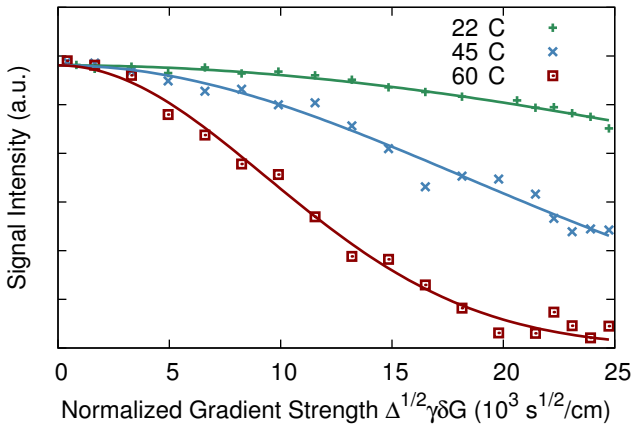

Figure 5.2: ^{7}Li PFGSE measurements of PEO/$LiClO_4$. The x-axis is normalized for the diffusion time Δ, gradient pulse duration δ, and gyromagnetic ratio γ.

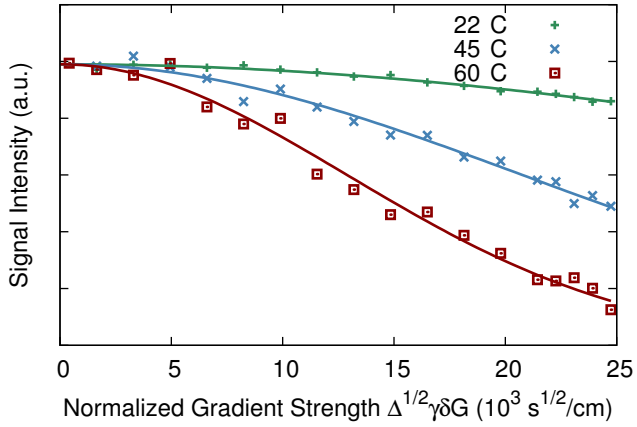

Figure 5.3: ^{7}Li PFGSE measurements of PEO/PEO-b(875)-PE/$LiClO_4$. The x-axis is normalized for the diffusion time Δ, gradient pulse duration δ, and gyromagnetic ratio γ.

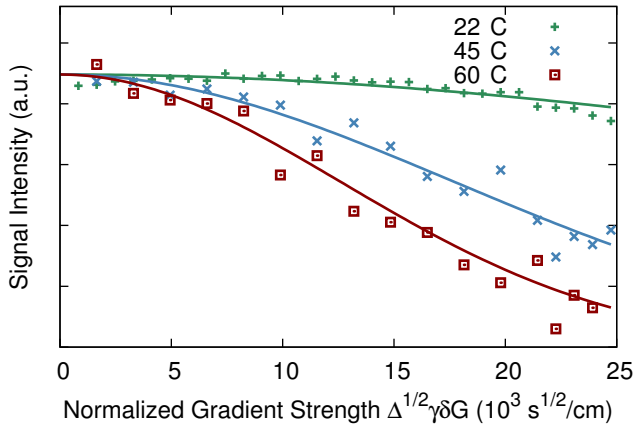

Figure 5.4: ^{7}Li PFGSE measurements of PEO/PEO-b(920)-PE/$LiClO_4$. The x-axis is normalized for the diffusion time Δ, gradient pulse duration δ, and gyromagnetic ratio γ.

The (875) sample was measured over a wider range of temperatures and the diffusion coefficient is plotted against temperature in Figure 5.5. The diffusion coefficient steadily increased up to the maximum temperature measured of 66°C.

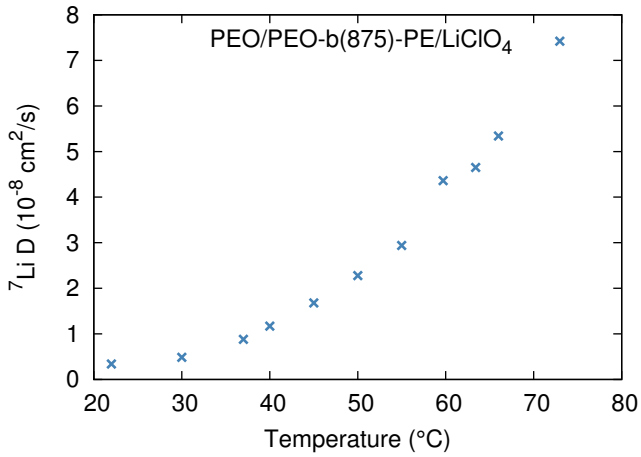

Figure 5.5: ^{7}Li diffusion coefficients of the PEO/PEO-b(875)-PE/$LiClO_4$ sample as a function of temperature.

Generally, the (920) and (875) samples demonstrated similar behaviour with temperature and had comparable diffusion coefficients. The largest diffusion coefficient at room temperature of 5.1x10^{-9} cm^2/s was obtained from the PEO/$LiClO_4$ sample with the (875) and (920) samples only a factor of 1.5 less. The lithium ion diffusion lengths at room temperature were on the order of approximately 0.80 μm to 1.0 μm, well within the thickness of the thin-polymer sample (~200 μm) and therefore unrestricted. With the increasing diffusion coefficients, we would also expect increased conductivity with temperature.

Since the reported conductivity of the (875) sample was 30x the conductivity of the (920) sample, the similar lithium cation diffusion coefficients suggest that this increase is not due to an increase in lithium cation mobility. If the concentrations of ^{7}Li in the samples were equal ($LiClO_4$ was intended to be 15 wt% in each of the samples.[11]), the increase must be due to increased dissociation or an increase in anionic mobility.

The diffusion coefficients in the dry PEO-b-PE polymers were greater than those of the dry AMLi/PEGDM 40/60 sample at a given temperature.

The PEO-b-PE samples had a ^{7}Li diffusion coefficient of ~4x10^{-8} cm^2/s near 60°C comparable with the AMLi/PEGDM 40/60 dry polymer ^{7}Li and ^{19}F diffusion coefficients of 3.4x10^{-8} cm^2/s and 2.2x10^{-8} cm^2/s at 100°C. The ClO_4^- anion in the block polymer was not measured, however it is expected that the anion would also be mobile and therefore the polymer electrolyte would have a low transference number compared to the transference number of t_+=1 attainable in a single-ion conducting polymer.

The reported conductivities by our collaborators were ~10^{-7} S/cm at 30°C for the AMLi X/Y dry samples and ~10^{-4} to 10^{-5} S/cm at room temperature for the PEO/PEO-b-PE/$LiClO_4$ dry samples. The faster cationic diffusion coefficients are consistent with these results. Diffusion coefficients in the PEO/PEO-b-PE/$LiClO_4$ samples were easily measured at room temperature, however, we were unable to measure diffusion in the dry AMLi/ PEGDM X/Y samples at room temperature.

As the anionic diffusion coefficient was not measured, it is only possible to approximate a calculated conductivity σ_{NMR} based on the cationic diffusion coefficient D_+. A density of 1.2 g/cm^3 was estimated for the sample in order to approximate a concentration of $LiClO_4$. σ_{NMR} was approximated as 2x10^{-5} S/cm at room temperature for the PEO/PEO-b(920)-PE/$LiClO_4$ sample. This is only 2x the reported conductivity measurements from Zhong's research group of 1.1x10^{-5} S/cm on a similar sample at room temperature[11], indicating a relatively high degree of dissociation. A numeric approximation of the percent dissociation would require the anionic diffusion coefficient, but would be a maximum of 55% based on only the cationic diffusion coefficient. Using the same approximations for the (875) sample, we find σ_{NMR} is an order of magnitude less than σ_{EXP} indicating a dissociation greater than 100%. Including the anionic diffusion coefficient would resolve this paradox but it is clear that the (875) sample must be highly dissociated compared to the (920) sample.

Mechanically, these materials were much more flexible and durable than the AMLi/PEGDM X/Y materials. The thin polymer membrane was easily rolled up and packed into the centre of the NMR sample tube. In comparison, the AMLi/PEGDM materials had to be carefully handled with tweezers and the more brittle samples had a tendency to break.

Overall the PEO/PEO-b-PE/$LiClO_4$ samples demonstrated higher ^{7}Li mobility and superior mechanical properties for a flexible polymer electrolyte. The drawbacks of a low transference number could be offset by the higher mobilities and increased conductivities and requires further investigation and analysis beyond our NMR characterization.

Chapter 6

Conclusion and Future Work

Lithium ion battery technology is currently used in the majority of mobile devices and is now being implemented in electric vehicles. The technology offers durability, high voltage, and a high power-to-weight ratio. However, there are still gains to be made in performance and safety, driving research and development for improved technology. Improving battery technology would open up opportunity for wider use in sustainable technologies such as electric vehicle applications. Additionally, higher energy density batteries could be used for improved mobile devices. Fundamental materials research will enable us to engineer materials leading to improved performance and safety of batteries.

Ultimately, any new material must be evaluated in the context of a complete battery cell. However, the electrolyte is one component where large performance and safety gains can be accomplished and we have concentrated our efforts on the characterization of isolated solid polymer electrolyte materials. Solid polymer electrolytes could improve on conventional liquid electrolytes with benefits including manufacturability and safety. These materials would function as both electrolyte and electrical separator between the anode and cathode and could have important advantages in manufacturing ultra thin, flexible, and lightweight battery cells. For practical implementation, the transport properties of these materials must be optimized so they are comparable to those of liquid electrolytes. Important transport properties include a high transport (or transference) number and high conductivity which are associated with the mobility of cationic and anionic species and depend on their diffusion coefficients. We have characterized two different solid polymer electrolyte materials.

The first material, AMLi/PEGDM, is a result of research efforts on single-ion conducting polymers. The material is meant to combine the high conductivity properties of ionic liquids with single-ion conduction. The goal of the synthesis was to produce a polymerized ionic liquid, where crosslinking immobilizes the fluorinated anionic species and the lithium cations are mobile. Our PFGSE NMR diffusion measurements have demonstrated that both the lithium cations and fluorinated anions are mobile and contribut-

ing toward conductivity. Therefore, further work is required to successfully immobilize the fluorinated anion in a crosslinked network. In particular, we have measured ^{7}Li and ^{19}F diffusion coefficients of 3.4x10^{-8} cm^2/s and 2.2x10^{-8} cm^2/s in the dry AMLi/PEGDM 40/60 sample at 100 °C. Furthermore, we have observed multi-component relaxation times. In the spectra, we observed a distinct broad Gaussian component, associated with low mobility and inconsistent with a homogeneous crosslinked polymer. The low mobility component decreased with increasing temperature, consistent with a gradual increase in conductivity observed in the AMLi/PEGDM samples.

A second generation of AMLi/PEGDM samples was synthesized in an effort to create polymer samples with an absence of uncrosslinked monomer, which may have contributed to the unexpected anionic diffusion results. However, anionic diffusion was also observed in these AMLi/PEGDM w/ DCPD samples. In order to quantify how much of the fluorine was contributing toward our diffusion results, PFGSE quantification experiments were performed. Quantification of diffusing species was accomplished by accounting for relaxation times in the PFGSE sequence. To validate the technique, we have measured a reference sample PEGM/PEGDM/LiTFSI, where the amount of lithium cations and fluorinated anions contributing to diffusion were in an equal ratio as expected. Furthermore, this homogeneous sample had single-component relaxation times and diffusion coefficients, in contrast to the AMLi/PEGDM X/Y samples. The technique was used to quantify the diffusion properties of AMLi/PEGDM 20/80 w/DCPD. The results indicated that fluorine and lithium quantities in the sample were in a ratio of 10.7, consistent with the very weak ^{7}Li signal in the sample. All of the fluorine was mobile. The fluorinated anion had two diffusing components with diffusion coefficients of 2.4x10^{-8} cm^2/s and 1.9x10^{-9} cm^2/s at 100 °C. 30% of the fluorinated anions were attributed to the slower diffusion component indicating that some of the fluorine may have been partially immobilized. The quantification study of this sample demonstrated inconsistent materials properties of those expected of a single-ion conducting polymer. The material did not appear to be successfully crosslinked and the amount of lithium left in this particular sample suggested that perhaps the majority of it had been removed unexpectedly in the synthesis. Further work in these AMLi/PEGDM samples is therefore required to successfully crosslink the sample and immobilize the fluorinated anionic components.

A second polymer electrolyte material PEO/PEO-b-PE/$LiClO_4$ is a result of research efforts to maximize conductivity and mechanical properties of a solid polymer electrolyte. The material was not intended to be single-ion conducting. ^{7}Li diffusion coefficients of these samples were higher than the

AMLi/PEGDM samples at a given temperature. The PEO/PEO-b(875)-PE/$LiClO_4$ and PEO/PEO-b(920)-PE/$LiClO_4$ samples had a ^{7}Li diffusion coefficient of ~4x10^{-8} cm^2/s near 60°C comparable with the AMLi/PEGDM 40/60 dry polymer ^{7}Li and ^{19}F diffusion coefficients of 3.4x10^{-8}cm^2/s and 2.2x10^{-8}cm^2/s at 100 °C. The ClO_4^- anion in the block polymer was not measured. However, it is expected that the anion would also be mobile in the sample consistent with a low cationic transference number (compared to a single-ion conducting polymer with t_+=1). The cationic diffusion coefficients were related to the reported conductivities using the Nernst-Einstein equation. Results demonstrated that the increase in conductivity between the (920) and (875) sample was not due to increased cationic mobility. Our results suggest the (875) sample had increased ionic dissociation and therefore more charge carriers contributing toward conductivity.

Overall the PEO/PEO-b-PE/$LiClO_4$ samples demonstrated higher ^{7}Li diffusion coefficients and superior mechanical properties for a flexible polymer electrolyte. The draw-backs of a low transference number could be offset by increased mobility and requires further investigation and analysis beyond our NMR characterization. The transport of these materials cannot be compared in the context of single-ion conduction versus bi-ionic conduction as the AMLi/PEGDM samples were not found to be single-ion conducting.

Continued work to develop polymer electrolytes is ongoing with our Cergy-Pontoise and Washington State Collaborators. For future measurements using the quantification technique the following recommendations follow from our study:

- Efforts should be made to keep the samples more uniform inside the RF coil for the best accuracy. One suggestion is to create indicators on the NMR glass sample holders, so that samples can be more easily aligned.

- Relatively strong signal strength is required for the quantification experiments. Efforts should be made to increase the signal strength in the sample by using a larger sample size. There is a competing issue that conductive samples load the RF coil causing difficulty in NMR measurements so the sample size should not be maximized, only increased.

- To obtain more accurate T_2 relaxation measurements in the PFGSE experiment, results should be compared by applying the gradient pulse at the beginning versus the end of the echo delay in the experiment. This would confirm the effect of eddy currents from the gradient coil.

Further PFG NMR experiments are planned to gain insight into new solid polymer samples under investigation. These measurements will continue to augment conductivity measurements and initial characterization. The author recommends transference number measurements of the polymer electrolytes that would provide a comparison to cationic and anionic diffusion coefficients. Generally, NMR measurements provide valuable insight into the transport mechanisms in these solid polymer materials and in particular, can confirm the mobility of individual cationic and anionic species.

Bibliography

[1] M. Lowe, S. Tokuoka, T. Trigg, and G. Gereffi, "Lithium-ion batteries for electric vehicles: The U.S. value chain," *Center on Globalization Governance and Competitiveness, Duke University*, 2010.

[2] A. Jossen, "Dynamics," in *Encyclopedia of Electrochemical Power Sources* (J. Garche, ed.), vol. 1, pp. 478–488, Amsterdam: Elsevier, 2009.

[3] Dell Support, "2006 Notebook Battery Recall." `http://support.dell.com/support/batteryrecall/index.aspx/en/main?c=us&l=en&s=gen`, 08 2006.

[4] Office of Information and Public Affairs, "News from US Consumer Product Safety Commision." `http://www.cpsc.gov/cpscpub/prerel/prhtml06/06245.html`, 08 2006.

[5] Office of Information and Public Affairs, "News from US Consumer Product Safety Commision." `http://www.cpsc.gov/cpscpub/prerel/prhtml09/09035.html`, 10 2008.

[6] R. Rosmarin, "Apple Joins Dell in Sony Battery Recall." `http://www.forbes.com/2006/08/24/apple-sony-batteries-cx_rr_0824apple.html`, 08 2006.

[7] M. Ue, "Electrolytes: Nonaqueous," in *Encyclopedia of Electrochemical Power Sources* (J. Garche, ed.), vol. 5, pp. 71–84, Amsterdam: Elsevier, 2009.

[8] M. B. Armand, P. G. Bruce, B. Forsyth, B. Scrosati, and W. Wieczorek, "Polymer electrolytes," in *Energy Materials* (D. W. Bruce, D. O'Hare, and R. I. Walton, eds.), ch. 1, pp. 1–31, Chichester, West Sussex: John Wiley Sons Ltd., 2011.

[9] S. Ng, M. Forsyth, M. Garcia, D. MacFarlane, and M. Smith, "A Nuclear Magnetic Resonance Study of 7Li Dynamics in Polyether-urethane

Based Solid Polymer Electrolytes," *Electrochimica Acta*, vol. 43, no. 10-11, pp. 1551 – 1556, 1998.

[10] J. Garche, ed., *Encyclopedia of Electrochemical Power Sources*, vol. 5. Amsterdam: Elsevier, 2009.

[11] J. Ji, J. Keen, and W.-H. Zhong, "Simultaneous improvement in ionic conductivity and mechanical properties of multi-functional block-copolymer modified solid polymer electrolytes for lithium ion batteries," *Journal of Power Sources*, vol. 196, no. 23, pp. 10163 – 10168, 2011.

[12] M. Salomon, "Electrolytes," in *Encyclopedia of Electrochemical Power Sources* (J. Garche, ed.), vol. 2, pp. 134–139, Amsterdam: Elsevier, 2009.

[13] P. G. Bruce and C. A. Vincent, "Steady state current flow in solid binary electrolyte cells," *Journal of Electroanalytical Chemistry and Interfacial Electrochemistry*, vol. 225, pp. 1 – 17, 1987.

[14] P. G. Bruce, *Solid State Electrochemistry*. Cambridge; New York, NY, USA: Cambridge University Press, 1995.

[15] D. Golodnitsky, "Electrolytes: Single lithium ion conducting polymers," in *Encyclopedia of Electrochemical Power Sources* (J. Garche, ed.), vol. 5, pp. 112–128, Amsterdam: Elsevier, 2009.

[16] C. Chauvin, F. Alloin, P. Judeinstein, D. Foscallo, and J.-Y. Sanchez, "Electrochemical and NMR characterizations of mixed polymer electrolytes based on oligoether sulfate and imide salts," *Electrochimica Acta*, vol. 52, no. 3, pp. 1240 – 1246, 2006.

[17] M. H. Levitt, *Spin dynamics : basics of nuclear magnetic resonance*. Hoboken, N.J.: Wiley, 2008.

[18] K. Hayamizu, S. Tsuzuki, S. Seki, Y. Ohno, H. Miyashiro, and Y. Kobayashi, "Quaternary Ammonium Room-Temperature Ionic Liquid Including an Oxygen Atom in Side Chain/Lithium Salt Binary Electrolytes: Ionic Conductivity and 1H, 7Li, and 19F NMR Studies on Diffusion Coefficients and Local Motions," *The Journal of Physical Chemistry B*, vol. 112, no. 4, pp. 1189–1197, 2008. PMID: 18179199.

[19] T. L. James, "Chapter 1 Fundamentals of NMR." Technical Report, Department of Pharmaceutical Chemistry at the University of California, San Francisco, CA 95143, USA, 1998.

[20] A. Abragam, *The principles of nuclear magnetism*. Oxford [Oxfordshire]: Clarendon Press ; Oxford University Press, 1961.

[21] S. Arumugam, J. Shi, D. P. Tunstall, and C. A. Vincent, "Cation and anion diffusion coefficients in a solid polymer electrolyte measured by pulsed-field-gradient nuclear magnetic resonance," *Journal of Physics: Condensed Matter*, vol. 5, no. 2, p. 153, 1993.

[22] M. Williamson, J. Southall, H. S. A. Hubbard, S. Johnston, G. Davies, and I. Ward, "NMR measurements of ionic mobility in model polymer electrolyte solutions," *Electrochimica Acta*, vol. 43, no. 10â"11, pp. 1415 – 1420, 1998.

[23] S. Panero, B. Scrosati, and S. Greenbaum, "Ionic conductivity and 7Li NMR Study of Poly(ethylene glycol) complexed with lithium salts," *Electrochimica Acta*, vol. 37, no. 9, pp. 1533 – 1539, 1992.

[24] K. J. Adamic, S. G. Greenbaum, K. M. Abraham, M. Alamgir, M. C. Wintersgill, and J. J. Fontanella, "Lithium-7 NMR study of polymer electrolytes based on composites of poly[bis((methoxyethoxy)ethoxy)phosphazene] and poly(ethylene oxide)," *Chemistry of Materials*, vol. 3, no. 3, pp. 534–538, 1991.

[25] F. Croce, S. D. Brown, S. G. Greenbaum, S. M. Slane, and M. Salomon, "Lithium-7 NMR and ionic conductivity studies of gel electrolytes based on polyacrylonitrile," *Chemistry of Materials*, vol. 5, no. 9, pp. 1268–1272, 1993.

[26] P. T. Callaghan, *Translational dynamics and magnetic resonance : principles of pulsed gradient spin echo NMR*. New York: Oxford University Press, 2011.

[27] C. S. Johnson and D. Wu, "Diffusion measurements by magnetic field gradient methods," in *Encyclopedia of Magnetic Resonance* (R. K. Harris, ed.), Chichester, UK: John Wiley & Sons, Ltd, Sept. 2011.

[28] W. S. Price, "Pulsed-field gradient nuclear magnetic resonance as a tool for studying translational diffusion: Part 1. basic theory," *Concepts in Magnetic Resonance*, vol. 9, no. 5, pp. 299–336, 1997.

[29] A. Einstein, "Über die von der molekularkinetischen theorie der wärme geforderte bewegung von in ruhenden flüssigkeiten suspendierten teilchen (english: On the movement of samll particles suspended in

stationary liquids required by the molecular-kinetic theory of heat)," *Annalen der Physik*, vol. 322, no. 8, pp. 549–560, 1905.

[30] M. J. Duer, *Introduction to solid-state NMR spectroscopy*. Oxford, UK; Malden, MA: Blackwell, 2004.

[31] J. Keeler, *Understanding NMR spectroscopy*. Chichester: John Wiley and Sons, 2010.

[32] E. O. Stejskal and J. E. Tanner, "Spin diffusion measurements: Spin echoes in the presence of a Time-Dependent field gradient," *The Journal of Chemical Physics*, vol. 42, no. 1, p. 288, 1965.

[33] E. Hahn, "Spin echoes," *Physical Review*, vol. 80, pp. 580–594, Nov. 1950.

[34] J. Mattiello, P. Basser, and D. Lebihan, "Analytical Expressions for the b Matrix in NMR Diffusion Imaging and Spectroscopy," *Journal of Magnetic Resonance, Series A*, vol. 108, no. 2, pp. 131 – 141, 1994.

[35] J. E. Tanner, "Use of the stimulated echo in NMR diffusion studies," *The Journal of Chemical Physics*, vol. 52, no. 5, p. 2523, 1970.

[36] W. Zhang and D. Cory, "Pulsed Gradient NMR Probes for Solid State Studies," *Journal of Magnetic Resonance*, vol. 132, no. 1, pp. 144 – 149, 1998.

[37] B. H. Suits and D. E. Wilken, "Improving magnetic field gradient coils for NMR imaging," *Journal of Physics E: Scientific Instruments*, vol. 22, pp. 565–573, Aug. 1989.

[38] C.-H. Tso, "NMR study of PF doped polypyrrole : a potential candidate for artificial muscles," Master's thesis, University of British Columbia, 2006.

[39] M. S. Conradi, A. Garroway, D. Cory, and J. Miller, "Generation of short, intense gradient pulses," *Journal of Magnetic Resonance (1969)*, vol. 94, no. 2, pp. 370 – 375, 1991.

[40] B. M. Braun and H. Weingaertner, "Accurate self-diffusion coefficients of lithium(1+), sodium(1+), and cesium(1+) ions in aqueous alkali metal halide solutions from NMR spin-echo experiments," *The Journal of Physical Chemistry*, vol. 92, pp. 1342–1346, Mar. 1988.

[41] C. A. Michal, K. Broughton, and E. Hansen, "A high performance digital receiver for home-built nuclear magnetic resonance spectrometers," *Review of Scientific Instruments*, vol. 73, no. 2, p. 453, 2002.

[42] J. Juger, F. Meyer, F. Vidal, C. Chevrot, and D. Teyssié, "Synthesis, polymerization and conducting properties of an ionic liquid-type anionic monomer," *Tetrahedron Letters*, vol. 50, pp. 128–131, Jan. 2009.

[43] A. K. Whittaker, "NMR studies of crosslinked polymers," in *Annual Reports on NMR Spectroscopy* (G. Webb and I. Ando, eds.), vol. 34 of *Annual Reports on NMR Spectroscopy*, pp. 105 – 183, Academic Press, 1997.

[44] J. Ji, B. Li, and W.-H. Zhong, "Simultaneously enhancing ionic conductivity and mechanical properties of solid polymer electrolytes via a copolymer multi-functional filler," *Electrochimica Acta*, vol. 55, no. 28, pp. 9075 – 9082, 2010.

[45] J. Ji, B. Li, and W.-H. Zhong, "Effects of a block copolymer as multifunctional fillers on ionic conductivity, mechanical properties, and dimensional stability of solid polymer electrolytes," *The Journal of Physical Chemistry B*, vol. 114, no. 43, pp. 13637–13643, 2010.